Coordination Chemistry Reviews 508 (2024) 215773

Contents lists available at ScienceDirect

Coordination Chemistry Reviews

journal homepage: www.elsevier.com/locate/ccr

Lanthanide-based nanoparticles for cancer phototherapy

Zichao Luo [a,b,*], Duo Mao [c], Xinchao Li [d], Jing Luo [b], Changyang Gong [d,*], Xiaogang Liu [b,*]

[a] Eye Institute and Department of Ophthalmology, Eye & ENT Hospital, Fudan University, NHC Key Laboratory of Myopia (Fudan University), Key Laboratory of Myopia, Chinese Academy of Medical Sciences, Shanghai Research Center of Ophthalmology and Optometry, Shanghai 200030, PR China
[b] Department of Chemistry and The N.1 Institute for Health, National University of Singapore, 117543, Singapore
[c] Institute of Precision Medicine, The First Affiliated Hospital of Sun Yat-sen University, Guangzhou, 510080, PR China
[d] State Key Laboratory of Biotherapy and Cancer Center, West China Hospital, Sichuan University, Chengdu 610041, PR China

ARTICLE INFO

Keywords:
Lanthanide-doped nanoparticles
Phototherapy
Immunotherapy
Cancer
Gene therapy

ABSTRACT

Phototherapy, using light as a therapeutic modality, has been widely applied in treating various diseases, especially cancer. This approach is valued for its non-invasive nature and minimal risk of drug resistance. However, phototherapy faces challenges such as the undesired delivery of phototherapeutic agents, potential phototoxicity, and limited penetration of light into tissues. Lanthanide-doped nanoparticles offer attractive opportunities to improve the therapeutic efficacy of photodynamic therapy. These nanoparticles are distinguished by their unique optical properties, such as excellent photostability against blinking and bleaching effects, large Stokes or anti-Stokes shifts, sharp emission peaks, and long luminescence lifetimes. In addition, lanthanide-doped nanoparticles can be excited by near-infrared (NIR) light or X-rays, enabling deep-tissue penetration. Beyond the use of photosensitizers, nanoparticle surfaces can be easily modified with targeting ligands, chemical drugs, or functional molecules to enhance the effectiveness of phototherapy or to enable combination therapy. In this review, we organize the use of lanthanide-based nanoparticles in tumor phototherapy into six main domains: photodynamic therapy, photothermal therapy, X-ray-based therapy, light-controlled therapy, photoimmunotherapy, and other innovative treatments that can be regulated by light. We introduce the basic principles of phototherapy and the characteristics of lanthanide nanoparticles. Following this, we summarize the latest advances in utilizing lanthanide-based nanoparticles for tumor phototherapy, focusing on their design principles, mechanisms of action, and effectiveness in cancer treatment. To conclude, we address the existing challenges and explore future opportunities within this area of research.

1. Introduction

Modern phototherapy dates back to 120 years ago [1]. In 1903, Niels Ryberg Finsen received the Nobel Prize in Physiology or Medicine for his work. He applied short-wavelength light to treat lupus vulgaris, which was considered the beginning of modern phototherapy [2]. Later, phototherapy based on eosin and white light was applied to treat skin tumors [1]. Recently, phototherapy has been widely employed to treat

Abbreviations: NIR, near-infrared; PDT, photodynamic therapy; PTT, photothermal therapy; ROS, reactive oxygen species; MOFs, metal-organic frameworks; LNPs, lanthanide-based nanoparticles; X-PDT, X-ray-induced photodynamic therapy; RT, radiotherapy; $O_2^{\bullet-}$, superoxide radicals; $HO^{\bullet}$, hydroxyl radicals; H_2O_2, hydrogen peroxide; $^1O_2$, reactive singlet oxygen; Ce6, chlorin e6; AIEgens, aggregation-induced emission luminogens; ZIF, zeolitic imidazolate framework; MIL, Materials Institute Lavoisier; APE1, apurinic/apyrimidinic endonuclease 1; PFCs, perfluorocarbons; Hb, hemoglobin; Dox, doxorubicin; PTA, photothermal agents; MRI, magnetic resonance imaging; CT, computed tomography; FRET, Förster resonance energy transfer; TiO_2, titanium dioxide; ZnO, zinc oxide; TLR, toll-like receptors; STING, stimulators of interferon genes; APCs, antigen-presenting cells; AMP, adenosine monophosphate; GMP, guanosine monophosphate; CTLA-4, cytotoxic T lymphocyte-associated antigen-4; ECM, extracellular matrix; IFP, interstitial fluid pressure; ICG, indocyanine green; TDPAs, tumor-derived protein antigens; CAR, chimeric antigen receptor; PEG, poly(ethylene glycol); NO, nitric oxide; siRNA, small interfering RNA; CRISPR, clustered regularly interspaced short palindromic repeats; sgRNA, single-guide RNA; MnO_2, manganese dioxide; Au_2O_3, gold trioxide; SPCD, silicon phthalocyanine dihydroxide; TPZ, tirapazamine; HIF-1a, hypoxia-inducible factor-1a; HA, hypocrellin A; H_2S, hydrogen sulfide; SO_2, sulfur dioxide; CO, carbon monoxide; MDR, multi-drug resistance; MC540, merocyanine 540; ZnPc, zinc phthalocyanine; ESA, excited state absorption; ETU, energy transfer upconversion; EMU, energy migration upconversion; CSU, cooperative sensitized upconversion; CR, cross-relaxation; PA, photon avalanche.

* Corresponding authors.
E-mail addresses: luozc@fudan.edu.cn (Z. Luo), gongchangyang@scu.edu.cn (C. Gong), chmlx@nus.edu.sg (X. Liu).

https://doi.org/10.1016/j.ccr.2024.215773
Received 2 December 2023; Accepted 27 February 2024
Available online 14 March 2024

various diseases, including atopic dermatitis, psoriasis, vitiligo, acne vulgaris, and cancer [3–8]. Phototherapy is considered a noninvasive therapeutic strategy with nondrug resistance compared with chemical therapy. Usually, phototherapy mainly consists of photodynamic therapy (PDT) and photothermal therapy (PTT). PDT utilizes the sensitized photosensitizers to produce reactive oxygen species (ROS) by the intersystem crossing to kill tumor cells. PTT experiences nonradiative decay to generate heat for destroying tumor cells. PDT has been applied in the clinic for over 40 years to treat various cancers, such as superficial skin lesions and oesophageal and lung tumors [9]. In contrast, PTT have not yet been used in clinical trials, but laser ablation without photothermal agents has been employed in the clinic.

Despite great progress in the clinic for tumor treatment, phototherapy still has not reached its full potential, owing to several existing challenges [9]. First, the low selectivity of PTT and PDT agents for tumor tissues over neighboring normal tissues requires a high dosage to assure an ideal therapeutic effect, resulting in high side effects. Additionally, the limited penetration of the excited light over biological tissues leads to an ineffective PTT or PDT on deep-seated tumors. Moreover, the hypoxic environment of tumor sites greatly restricts the therapeutic efficacy of PDT since this therapeutic effect is oxygen-dependent. Furthermore, potent 'dark toxicity' associated with the undesired excitation of residual photosensitizers also limits the clinical application of PDT.

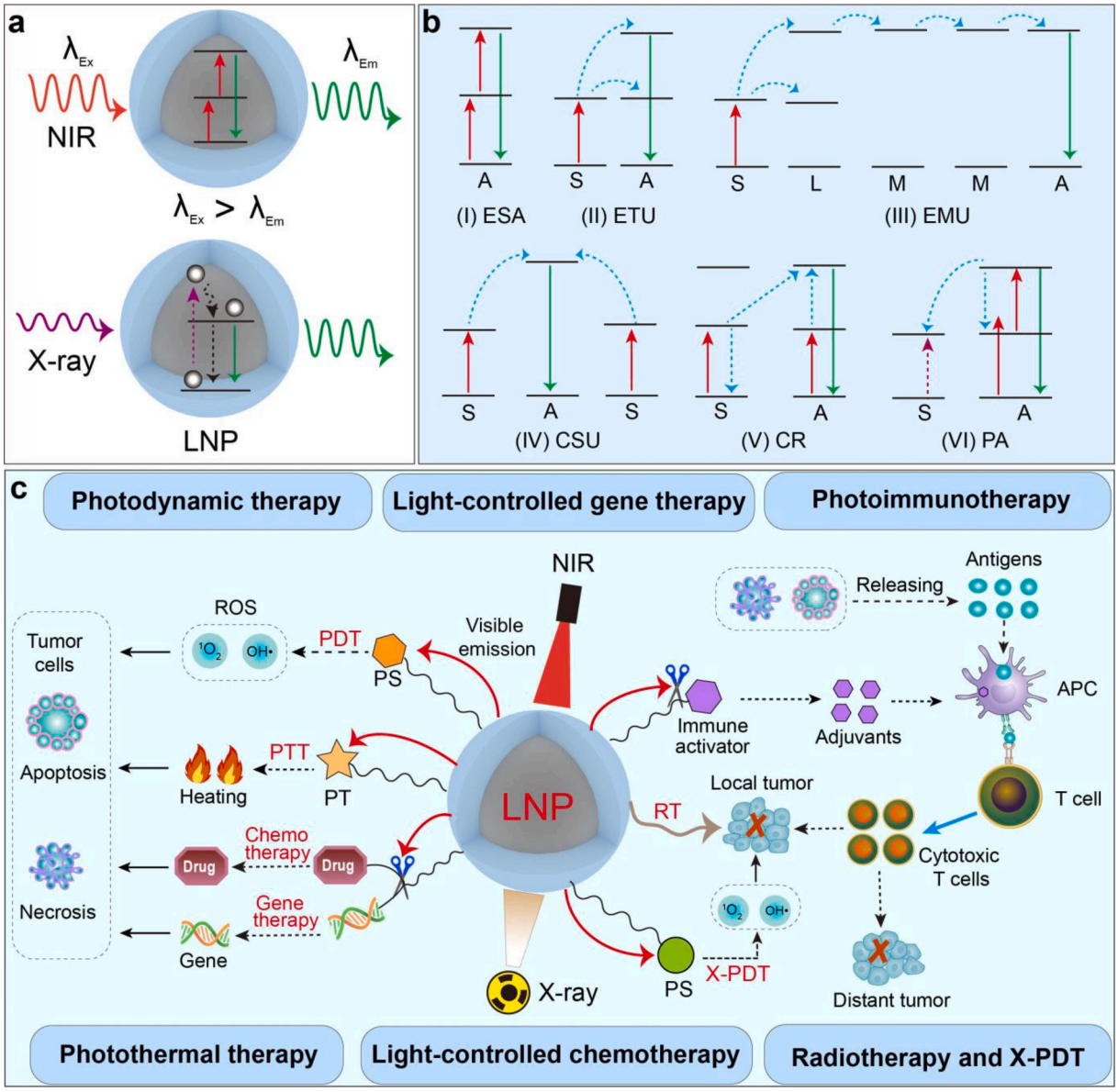

Fig. 1. Diverse applications of lanthanide-based nanoparticles (LNPs) in cancer treatments. (**a**) Schematic of a core–shell-structured upconversion nanoparticle exhibiting typical anti-Stokes emission with photon energy higher than that of the excitation light ($\lambda_{ex} > \lambda_{em}$) (top); and the typical nonradiative and radiative decays of lanthanide nanoparticles under X-ray irradiation (bottom). (**b**) Principal upconversion mechanisms of lanthanide-doped nanoparticles. ESA, excited state absorption; ETU, energy transfer upconversion; EMU, energy migration upconversion; CSU, cooperative sensitized upconversion; CR, cross-relaxation; PA, photon avalanche; S, sensitizer; A, activator; L, energy ladder; M, energy migratory ion. (**c**) Key tumor therapy methods utilizing LNPs, including photodynamic therapy (PDT), photothermal therapy (PTT), photoimmunotherapy, radiotherapy (RT), light-regulated chemotherapy/gene therapy, and X-ray-induced photodynamic therapy (X-PDT). When activated by near-infrared light or X-rays, LNPs can stimulate photosensitizers (PS), photothermal agents (PT), or catalysts and initiate the production of reactive oxygen species (ROS) or the release of chemical drugs or genes. These productions can induce apoptosis of tumor cells, thus inhibiting local tumor growth. In combination with tumor antigens released from these dead tumor cells, LNPs loaded with immune activators can promote antigen presentation by inducing maturation of antigen-presenting cells (APCs), and subsequently boost strong cellular immune responses, thereby inhibiting distant tumor growth.

To improve the antitumor performance of phototherapy, a variety of nanomaterials have been developed, such as micelles, liposomes, dendrimers, metal oxide nanoparticles, quantum dots, silica nanoparticles, upconversion nanoparticles, metal–organic frameworks (MOFs) and so on [10–12]. These nanomaterials potently enhance their therapeutic efficacy due to their distinguishing characteristics, including tunable size, high therapeutic agent loading, high tumor-targeting ability, good biocompatibility, and modifiable surfaces [13]. Among these nanoparticles, lanthanide-based nanoparticles (LNPs) are emerging as promising nanoplatforms for enhanced phototherapy owing to their unique optical properties such as narrow-band emission, super photostability, high emission efficacy, and long emission lifetime [14–16]. Another notable optical feature of LNPs that enhances phototherapy is the upconversion process. This process allows for the conversion of ultraviolet-to-visible emission (400–750 nm) through radiative transitions upon near-infrared (NIR) excitation (e.g., 808 and 908 nm, Fig. 1a) [17]. The mechanisms of upconversion emission in lanthanide ions can be mainly categorized into six types: excited state absorption (ESA), energy transfer upconversion (ETU), energy migration upconversion (EMU), cooperative sensitized upconversion (CSU), cross-relaxation (CR), photon avalanche (PA) (Fig. 1b). Beyond upconversion, LNPs are capable of down-conversion emission under NIR irradiation, known as the Stokes shift [18]. This leads to emitted light with a longer wavelength (lower energy) than the absorbed light, resulting in second near-infrared (NIR-II) luminescence, ideal for deep-tissue bio-imaging. Furthermore, the ability of LNPs to be activated by NIR light facilitates deep-tissue tumor therapy with minimal phototoxicity and enables NIR-dependent delivery of chemical drugs, genes, or antibodies.

In addition to their robust response to NIR light, LNPs also exhibit high responsivity to X-rays due to the high atomic number (high-Z) radiosensitization properties of lanthanide ions. LNPs, when stimulated with X-rays, can absorb and scatter X-ray energy, leading to X-ray attenuation [19]. The scattered energy may be absorbed by nearby tumor tissues, rendering LNPs effective radiosensitizers for enhanced cancer radiotherapy (RT). Moreover, LNPs can absorb X-ray photons and convert them into UV–visible luminescence through radiative decay pathway (Fig. 1a), providing a novel approach to tumor therapy known as X-ray-induced photodynamic therapy (X-PDT). Furthermore, the surface modification of LNPs with different targeting ligands or functional moieties can improve tumor targeting and facilitate combined oncological treatments, including PDT with immunotherapy or gene therapy.

Despite the vast number of publications covering the bio-applications of LNPs over the past decade, which mainly focus on their synthesis, optical properties, and general applications in biomedical imaging and therapeutics [14,20,21], most reviews have concentrated on one or two specific types of LNP-based cancer phototherapies, such as PDT, PTT, radiotherapy, or combined PDT/PTT therapy [19,22–24]. However, recent advances have introduced promising LNP-based cancer phototherapy, including light-triggered gas therapy, non-oxygen free radical therapy, and electron interference therapy. This review aims to cover the recent progress in LNP-based phototherapy in a broader context, including PDT, PTT, light-controlled chemical therapy, light-controlled gene therapy, radiotherapy, X-ray PDT, photo-immunotherapy, and other innovative light-triggered cancer treatments (Fig.1c). The discussion also extends to future challenges and prospects in LNP-based phototherapy.

2. Tumor photodynamic therapy

Photodynamic therapy develops its cytotoxic effect on tumor cells through reactive oxygen species (ROS). PDT consists of three critical elements: photosensitizer, light source, and molecular oxygen. Upon light irradiation, the photosensitizer can absorb photons and reach an electronically excited singlet state. Subsequently, the short-lived, excited singlet state can undergo intersystem crossing and then transition to a long-lived, electronically excited triplet state, emitting energy in the form of fluorescence, heat, or other form of photophysical energy. The long-lived triplet state subsequently facilitates the production of ROS through two pathways. In the type I pathway, the excited photosensitizer participates in an electron transfer reaction to produce free radicals and radical ions (e.g., superoxide radicals $O_2^{-}\bullet$, hydroxyl radicals $HO^{-}\bullet$, and hydrogen peroxide H_2O_2), while in the type II pathway, the photosensitizer transfers energy directly to molecular oxygen (O_2) to generate highly reactive singlet oxygen ($^1O_2$) (Fig. 2a). The ROS generated during type I and type II reactions can induce oxidative damage to tumor cells and ultimately lead to cell death [9]. Despite the potential for clinical success, the current state of PDT face limitations in therapeutic efficacy due to several factors: the shallow penetration of light into tissues, the low production of ROS by the photosensitizer, and low oxygen concentration in the targeted area. In this section, we focus on recent advances in improving PDT efficacy using LNPs. The emphasis is on strategies aimed at increasing the production of ROS while minimizing phototoxicity during PDT.

2.1. The light source

Most current clinical photosensitizers absorb light in the visible range (400–700 nm), which can penetrate around 3.5 mm into the tissue, making clinical PDT suitable for superficial tumors [25]. In contrast, LNPs can be stimulated by NIR light to emit visible light that propagates 5–10 mm into the tissue (Fig. 2b). Thus, the NIR-excited PDT technology based on LNPs can significantly improve treatment efficacy, especially for deep-seated tumors. For instance, nanocomposites based on $NaYF_4$:Yb/Er@$NaYF_4$ nanoparticles conjugated with Killer Red dyes achieved a 10-fold increase in PDT efficacy at ~ 1 cm tissue depth under 980 nm irradiation, compared to conventional Killer Red-based PDT under 580 nm irradiation [26]. Upon NIR light excitation, such Yb/Er-doped upconversion nanoplatforms loaded with other PS types, such as chlorin e6 (Ce6), titanium dioxide (TiO_2), merocyanine 540 (MC540), rose bengal, or zinc phthalocyanine (ZnPc), also achieved deep-penetrating PDT in various tumors covered with 8-mm or 10-mm-thick pork tissue [27–30].

In addition to the NIR-I window (980 nm or 808 nm), the NIR-II window can also activate LNPs to emit UV/visible light for PDT. For instance, a NIR-II (1532 nm)-responsive PDT nanoplatform was constructed by loading zinc phthalocyanine onto $NaLuF_4$:Er/Mn@$NaYF_4$@SiO_2 nanoparticle surfaces [31]. When irradiated at 1532 nm, this nanoplatform showed efficient antitumor growth *in vivo*, with deeper tissue-penetration compared to irradiation with a 980 nm or 1064 nm laser (Fig. 2c). Another NIR-II-light activated PDT for the treatment of Panc-1 tumors with deep-tissue penetration was achieved by silica-coated $LiYbF_4$:Er @$LiGdF_4$ nanoparticles loaded with rose bengal and Ce6 under 1550 nm irradiation [32].

2.2. The photosensitizer

The tunability of upconverting photoluminescence in LNPs can be achieved by adjusting lanthanide ion concentrations or constructing different core–shell structures. One strategy to improve the therapeutic efficacy of LNP-based PDT involves aligning the upconverted emission peak of LNPs and the absorption band of photosensitizers, maximizing their activation. In 2018, He *et al.* developed a $NaErF_4$@$NaLuF_4$-based PDT platform displaying spectral overlap between nanoparticle red emission (650 nm) and zinc phthalocyanine photosensitizer absorption upon 808 nm excitation [33]. When irradiated with an 808 nm laser at a low power density (0.6 W/cm^2) for 5 min, this platform effectively suppressed 65 % tumor cell growth in the Hela cell spheroid model, indicating efficient PDT without thermal effects.

Loading nanoparticle surfaces with two types of photosensitizers is another strategy to improve PDT efficacy. This approach leverages multicolor emission from LNPs to activate all photosensitizers

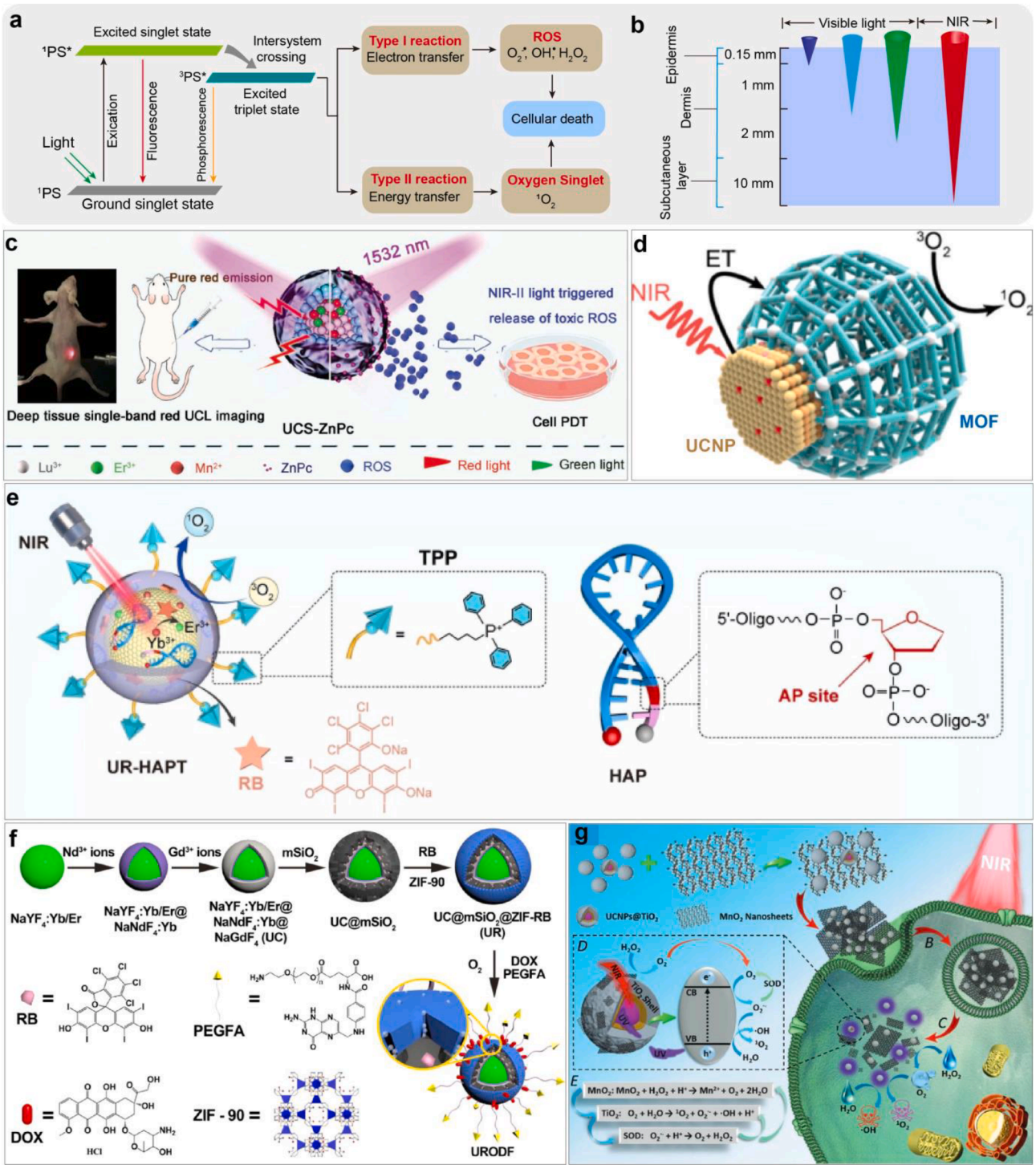

Fig. 2. Various applications of lanthanide-based nanoparticles (LNPs) in tumor photodynamic therapy (PDT). (a) Mechanism of PDT involving photosensitizer (PS) excitation. (b) Tissue penetration by visible to NIR light. c) NIR-II-responsive upconversion nanoparticles (UCNPs) utilized for PDT. Reproduced with permission from Ref. [31]. Copyright 2023 Wily-VCH Verlag GmbH & Co. KGaA. (d) Design of heterodimers involving a UCNP and a metal–organic framework for PDT. Reproduced with permission from Ref. [38]. Copyright 2017 American Chemical Society. (e) UCNP-based PDT targeting mitochondria, while imaging the enzymatic dynamics of APE1. Reproduced with permission from Ref. [46]. Copyright 2022 Wily-VCH Verlag GmbH & Co. KGaA. (f) Diagram illustrating pH-responsive nanoprobes loaded with oxygen, utilizing UCNPs coated with ZIF-90 MOF to overcome hypoxia during PDT. Reproduced with permission from Ref. [42]. Copyright 2019 American Chemical Society. (g) Nanocomposites generating oxygen, consisting of UCNP@TiO_2 and MnO_2 nanosheets for ROS-amplified PDT. Reproduced with permission from Ref. [51]. Copyright 2017 Wily-VCH Verlag GmbH & Co. KGaA.

simultaneously, thus improving ROS generation. For example, mesoporous silica-coated $NaYF_4$:Yb/Er/Nd@$NaYF_4$:Nd nanoparticles, loaded with ZnPc and MC540, showed a synergistic PDT effect against prostate cancer upon 980 nm laser irradiation [34]. Similarly, co-conjugating PSs from MC540 and ZnPc on nanoparticle surfaces upon 808 nm excitation yielded a synergistic PDT effect [35]. Likewise, employing amphiphilic polyethylene glycol polymers (DSPE-PEG_{2000}) conjugated with two photosensitizers, Ce6 and rose bengal, encapsulated $NaYF_4$:Yb/Er/

Nd@$NaYF_4$:Yb/Nd nanoparticles for enhanced PDT and enabled a synergistic effect in tumor eradication [36].

High doses of photosensitizers can hinder PDT efficacy by causing luminescence quenching. Aggregation-induced emission luminogens (AIEgens) offer a solution by showing strong emission upon aggregation. A nanoplatform combining $NaYF_4$:Yb/Tm/Nd@$NaYF_4$:Nd nanoparticles and AIEgens in DSPE-PEG nanomicelles demonstrated effective ROS generation, significantly suppressing tumor growth upon 808 nm irradiation [37]. Constructing heterostructure nanoparticles from LNPs and metal–organic frameworks (MOFs) is another strategy to enhance ROS generation without self-quenching. For example, in 2017, Li *et al.* developed heterostructural nanodimers from $NaGdF_4$:Yb/Er@$NaGdF_4$ nanoparticles and Zr-based porphyrinic MOFs for NIR-induced cancer PDT [38]. After irradiation at 980 nm, the heterodimer can facilitate singlet oxygen, production, resulting in potent inhibition of 4 T1 breast tumor growth *in vivo* (Fig. 2d). Various LNP@MOF nanocomposites, such as zirconium metalloporphyrin-based porous coordination network-222 (PCN-222), PCN-224, zeolitic imidazolate framework (ZIF)-8, ZIF-90, and Materials Institute Lavoisier (MIL)-100 (Fe), displayed significant antitumor effects upon NIR irradiation [39–43].

The extended diffusion of ROS before reaching intracellular organelles can actually decrease the cytotoxic impact on tumor cells. This occurs because ROS have a relatively short lifespan [44]. To enhance therapeutic efficacy, surface-modified LNPs with mitochondria-targeting ligands reduce ROS diffusion, leading to apoptosis of tumor cells. Nd^{3+}-doped upconversion nanoprobes functionalized with triphenylphosphine (TPP) exhibited potent tumor growth inhibition upon 808 nm irradiation [45]. In 2022, Yu *et al.* developed a multifunctional nanoplatform by conjugating mitochondria-targeting molecules (TPP) on $NaGdF_4$:Yb/Er@$NaGdF_4$ nanoparticles via an apurinic/apyrimidinic endonuclease 1 (APE1)-responsive DNA reporter [46]. The mitochondria-targeted platform showed a stronger antitumor effect upon NIR irradiation than the non-targeted nanoprobe upon NIR irradiation. Meanwhile, it provided real-time evaluation of PDT efficacy by imaging the dynamics of the cellular APE1 enzyme (Fig. 2e).

Direct triplet energy transfer from lanthanide ions to organic photosensitizers is another promising strategy. In 2021, Zheng *et al.* developed NIR photosensitization by coupling $NaGdF_4$:Nd nanoparticles with organic photosensitizers to produce ROS at ultralow NIR irradiance [47]. This platform generated a more than 100-fold higher level of ROS compared with conventional upconversion-based photosensitization systems and enabled significant tumor growth inhibition at low NIR irradiance (80 mW/cm^2), even when covered with a 4-mm pork tissue.

2.3. The oxygen

The hypoxic conditions in tumor microenvironments weaken the effectiveness of oxygen-dependent PDT. To overcome this challenge, two main strategies have emerged. LNPs serve to deliver both photosensitizers and oxygen carriers, such as perfluorocarbons (PFCs), hemoglobin (Hb), red blood cells, and MOFs. These carriers bind and release large amounts of oxygen into the tumor [48]. For instance, Wang *et al.* developed a microcarrier consisting of DSPE-PEG-modified red blood cells and an upconversion nanoparticle-based probe for hypoxia tumor therapy [49]. Under 808 nm or 980 nm irradiation, this microcarrier enabled efficient PDT by triggering substantial O_2 release from red blood cells. In 2019, Xie *et al.* introduced a multifunctional nanodrug carrier combining $NaYF_4$:Yb/Er@$NaYbF_4$:Nd@$NaGdF_4$ nanoparticles, zeolitic imidazolate framework-90 (ZIF-90) with mesoporous SiO_2 coating, rose bengal, and doxorubicin (Dox), and poly(ethylene glycol)-modified folic acid [42]. The mesoporous SiO_2-coated ZIF-90 serves as an O_2 reservoir, quickly releasing O_2 in tumor sites (pH 5.5). This mechanism enhanced the combined effect, effectively suppressing 4 T1 tumor growth *in vivo* (Fig. 2f).

In addition to oxygen-carrying agents, oxygen-generating agents can be co-delivered with photosensitizers by LNP to enhance PDT. Agents like manganese dioxide (MnO_2), gold trioxide (Au_2O_3), catalase-like nanoenzymes, MOFs, or ferric iron can catalyze H_2O_2 into water and O_2 at tumor sites [48]. For example, mesoporous cerium oxide modified with Yb/Tm-doped nanoparticles, Dox, and Arg-Gly-Asp (RGD)-peptides increased ROS generation, enhancing U87MG tumor cell death by around 30 % upon 980 nm irradiation [50]. In 2017, Zhang *et al.* devised multifunctional nanocomposites that consist of TiO_2-coated $NaYF_4$:Yb/Tm@$NaYF_4$ nanoparticles and MnO_2 nanosheets for oxygen-dependent PDT [51]. The MnO_2 nanosheet elevated ROS production by catalyzing intracellular H_2O_2 into O_2, improving tumor-killing by about 20 % under hypoxia conditions (Fig. 2 g). In 2023, Chen *et al.* constructed a NIR-regulated PDT nanoplatform, comprising $NaErF_4$:Tm@$NaYF_4$ nanoparticles with a porphyrin-based MOF shell, platinum nanoparticles, and mitochondria-targeting triphenylphosphine molecules. Upon NIR irradiation, this platform effectively attenuated tumor hypoxia through platinum nanoparticle-mediated oxygen generation, enhancing ROS generation and *in vivo* PDT efficacy [52].

The antitumor efficacy of PDT can be improved by employing LNPs to co-deliver bioreductive drugs to hypoxic regions within tumors. Bioreductive drugs that are activated in tumor cells under low oxygen conditions can produce a synergistic antitumor effect. For instance, in 2015, Liu *et al.* designed an upconversion nanoplatform with a double silica coating that can carry both silicon phthalocyanine dihydroxide (SPCD) and the bio-reductive pro-drug tirapazamine (TPZ) to enable combined tumor therapy [53]. This nanoplatform produced a large amount of ROS upon 980 nm irradiation and induced a hypoxia condition, promoting direct destruction of tumor cells by ROS and activating TPZ for bio-reductive therapy. This approach demonstrated a significant synergistic *in vivo* antitumor effect in a HeLa tumor model and outperformed LNP-mediated PDT alone. More recently, in 2022, Chen *et al.* developed a ROS-responsive upconversion nanoprobe consisting of silica-coated $NaYF_4$:Yb/Er@$NaYF_4$ nanoparticles, Ce6, doxorubicin, and Fe^{2+}, designed for enhanced PDT [54]. This nanoprobe not only directly eliminated MDA-MB-231 tumor cells by ROS under 980 nm irradiation, but also triggered the release of DOX and Fe^{2+}, leading to additional tumor cell death through DNA damage and the Fenton reaction, thereby achieving a synergistic effect through LNP-mediated PDT in combination with ROS-activated chemo and chemodynamic therapy.

Despite great progress, LNP-based PDT encounters limitations: low efficacy on large tumors; challenging treatment of metastatic cancers, complex nanocomposite preparation, and lacking comprehensive biosafety assessment for clinical use.

3. Tumor photothermal therapy

Photothermal therapy (PTT) relies on specific wavelength light to trigger excited electrons in photothermal agents (PTA) to release energy non-radiatively, raising the local tissue temperature (over 42 °C) and causing tumor cell death [9]. Despite its moderate effectiveness in inhibiting tumors, PTT often fails to completely eliminate tumor lesions due to several reasons: i) the limited depth at which visible-range light penetrates (wavelength of 400–700 nm); ii) the suboptimal performance and compatibility of current photothermal agents (PTAs); iii) inevitable heat damage to nearby normal tissues surrounding tumor lesions [55].

LNPs have great utility in enhancing the efficacy of PTT through enhanced heat production, leveraging their unique features, including stable fluorescence, tunable emission spectrum, temperature-responsive emission bands, and the ability for near-infrared excitation [56]. They are commonly paired with organic or inorganic photothermal agents (e.g., indocyanine green dye, polydopamine, or Prussian blue). This combination significantly increases the temperature in the surrounding tumor tissues, enhancing the effectiveness of the PTT. For instance, Liu *et al.* developed a nanoprobe based on polydopamine-coated $NaYF_4$:Yb/Er@$NaYF_4$:Yb nanoparticles loaded with indocyanine green molecules, resulting in enhanced PTT through both photothermal effects and ROS generation upon 808 nm laser irradiation [57]. In 2018, Li *et al.* designed

a core–shell nanoplatform ($NaLuF_4$:Gd/Yb/Er NRs@PDA) with polydopamine coating, displaying a high photothermal conversion efficiency of around 40 % [58]. In 2019, Wang *et al.* constructed a nanoplatform encapsulating prussian blue-coated $NaErF_4$@$NaYF_4$@$NaNdF_4$ nanoparticles within phospholipid PEG-based micelles, achieving remarkable tumor ablation upon 808 nm irradiation (Fig. 3a-e) [59].

Furthermore, combining LNPs with inorganic nanoparticles such as Au, Ag, Fe_3O_4 and CuS nanoparticles have been widely explored for

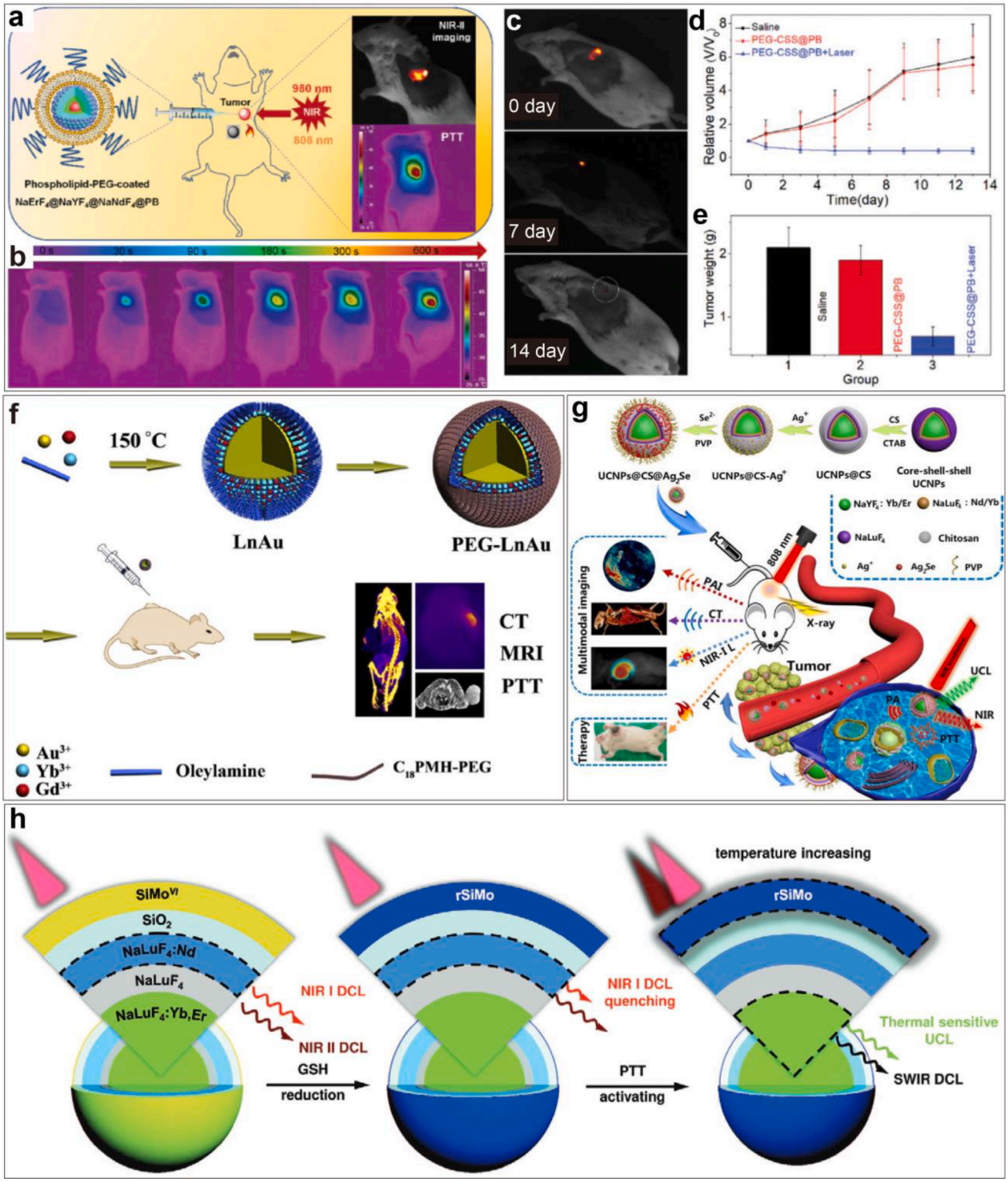

Fig. 3. LNP-based photothermal therapy and real-time temperature monitoring. (**a**) Design of phospholipid-PEG-coated nanopaltform used in photothermal therapy. (**b**) Thermographic images of tumor-bearing mice undergoing nanopaltform-mediated PTT. (**c**) NIR-II imaging of tumor-bearing mice at different intervals post photothermal therapy. (**d**, **e**) Average tumor volume and weight in the three groups of treated BALB/c mice. Reproduced with permission from Ref. [59]. Copyright 2019, The Royal Society of Chemistry. (**f**) Synthesis of amphiphilic polymer (C18MH-mPEG)-coated Gd/Yb-functionalized gold nanoparticles and their applications in multimodal imaging. Reproduced with permission from Ref. [65]. Copyright 2016, Elsevier Ltd. (**g**) Synthesis of UCNP@CS@Ag_2Se nanocomposites and their use in PTT. Reproduced with permission from Ref. [66]. Copyright 2019, Elsevier Ltd. (**h**) Glutathione (GSH)-activatable Er/Nd-doped core–shell-shell lanthanide nanoparticles tailored for PTT. Reproduced with permission from Ref. [70]. Copyright 2021, Wiley-VCH Verlag GmbH & Co. KGaA.

highly efficient PTT due to their high photothermal conversion efficiency and ease of synthesis and modification [60–64]. For instance, Ge *et al.* prepared a multifunctional nanoplatform using PEGylated amphiphilic polymer (C18MH-mPEG) on Gd/Yb-functionalized gold nanoparticles, demonstrating effective magnetic resonance imaging (MRI) and computed tomography (CT) imaging-guided PTT [65]. The nanoplatform exhibited a concentration-dependent temperature increase under 808 nm irradiation *in vitro* and exemplary performance in MR imaging and CT imaging-guided PTT in HeLa tumor-bearing mice (Fig. 3f). Another theranostic nanoprobe was developed by growing ultrasmall Ag_2Se nanodots on chitosan-coated $NaYF_4$:Yb/Er@$NaLuF_4$:Nd/Yb@$NaLuF_4$ nanoparticles, showcasing tetra-modal imaging-guided tumor PTT with minimal toxicity *in vivo* (Fig. 3 g) [66].

Accurate temperature measurement is essential in tumor treatment, particularly during PTT, where tumor temperatures undergo significant changes [67]. LNP-based luminescence thermometry offers real-time thermal imaging within tumors, minimizing overheating side effects. In 2016, Carrasco *et al.* designed Nd^{3+}-doped LaF_3 nanocrystals for controlled PTT in breast cancer, exhibiting *in vivo* photothermal effects that inhibited tumor growth [68]. These nanocrystals enabled intratumoral temperature measurements, paving the way for clinical use by showing distinct differences between intratumoral and skin temperatures. Another upconversion nanoprobe, using carbon-coated core–shell $NaLuF_4$:Yb/Er@$NaLuF_4$ nanoparticles, effectively monitored temperatures during PTT, achieving tumor ablation with minimal normal tissue damage [69]. In 2021, Liu *et al.* crafted glutathione-activatable, Er^{3+}/Nd^{3+}-doped core–shell-shell nanoparticles for thermally controlled PTT of subcutaneous orthotopic cancer [70]. Their approach significantly reduced tumor size under 808 nm irradiation compared with the control group. Moreover, these nanoprobes could provide real-time feedback of intrinsic temperature, enabling accurate irradiation of tumor sites without damaging peripheral normal breast tissues (Fig. 3 h).

LNPs have significantly enhanced traditional PTT by improving photothermal conversion efficiency and minimizing damage to adjacent normal tissues. However, challenges persist, including limited NIR penetration, inefficient upconversion efficacy due to multiphoton non-radiative transitions, and energy loss between nanoparticle emission and absorption by photothermal agents.

4. Tumor radiotherapy

Lanthanide-doped nanomaterials, which incorporate high atomic number elements, are highly valued for their strong X-ray absorption capabilities. This trait make them highly applicable in fields such as radiation detection, radiotherapy, and X-PDT [71]. X-rays can directly damage cellular DNA, leading to cell death *via* necrosis or apoptosis (Fig. 4a). As effective radiosensitizers, LNPs can intensify localized X-ray doses at tumor sites through the Compton scattering effect. This process facilitates the production of a significant number of electrons that directly damage DNA and generate ROS [19]. Moreover, LNPs can enhance the therapeutic efficacy of X-PDT by absorbing or storing X-rays and thereby boosting ROS generation, which primarily triggers tumor

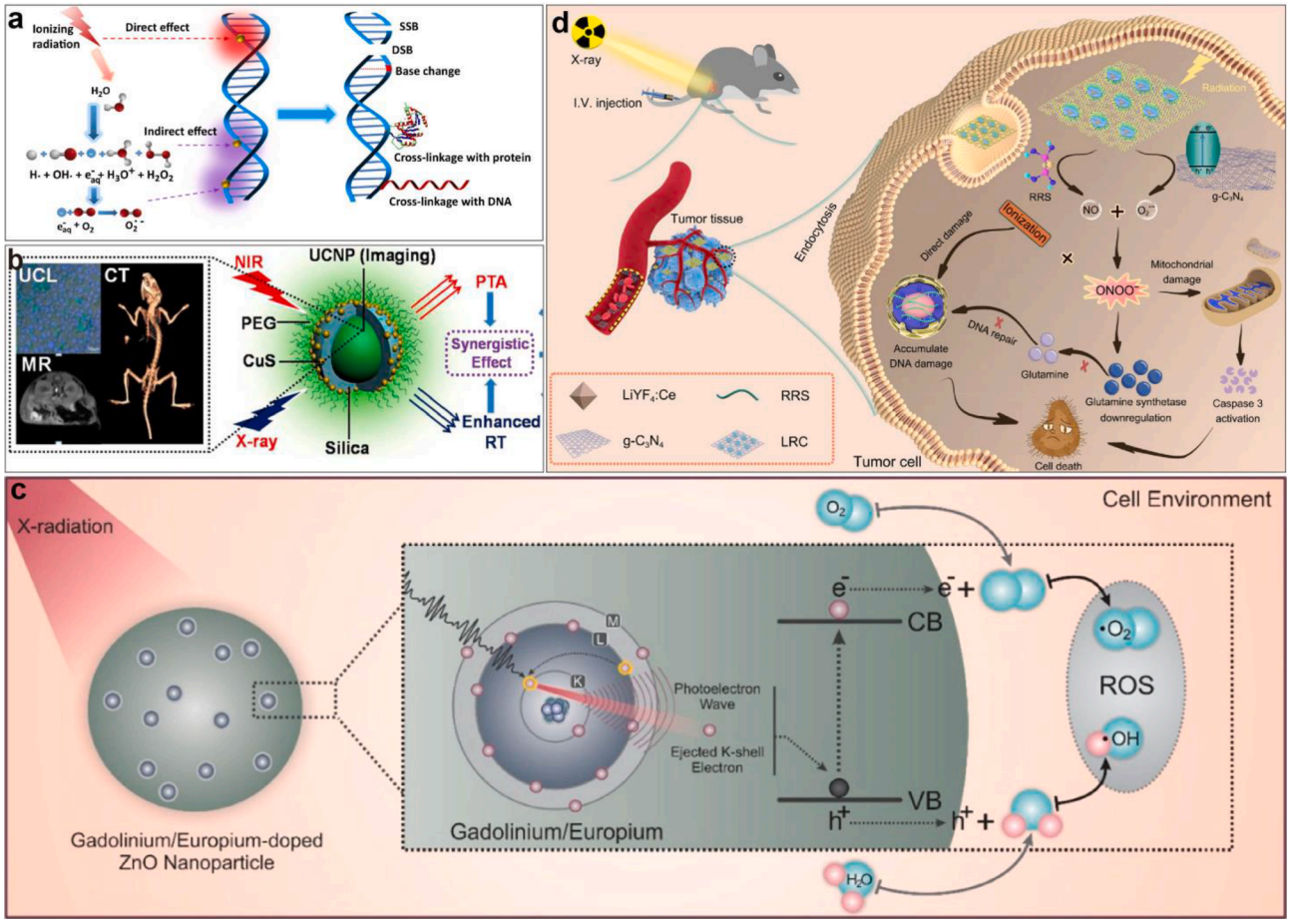

Fig. 4. LNP-based radiotherapy and photodynamic therapy. (**a**) Primary mechanisms of tumor cell death induced by X-rays, including direct and indirect pathways. Reproduced with permission from Ref. [71]. Copyright 2017 Elsevier Ltd. (**b**) Upconversion nanoparticle-based cancer radiotherapy combined with multi-model imaging. Reproduced with permission from Ref. [63]. Copyright 2013 American Chemical Society. (**c**) Gd- or Eu-doped ZnO nanoparticles used for X-ray-induced photodynamic therapy. Reproduced with permission from Ref. [84]. Copyright 2016 American Chemical Society. (**d**) Nanoscintillators generating peroxynitrite ($ONOO^-$) for tumor radiotherapy. Reproduced with permission from Ref. [88]. Copyright 2022 American Chemical Society.

cell apoptosis [72].

4.1. Radiotherapy

LNPs, owing to their strong X-ray absorption and scattering capabilities, serve as effective sensitizers in radiotherapy. For example, gadolinium (Gd)-based nanoparticles significantly induced apoptosis in radio-resistant U87 tumor cells when exposed to X-ray irradiation [73]. In 2013, Xiao *et al.* developed lanthanide-based radiosensitizers by coating ultra-small CuS nanoparticles onto silica-coated $NaYbF_4$:Er/Gd nanoparticles [63]. The presence of high-Z elements (Yb, Er and Gd) in these radiosensitizers could cause a deposition of X-ray energy and subsequently increase the local radiation dose around the tumor tissue, inducing highly apoptosis of tumor cells. This radiosensitizer-mediated radiotherapy enhanced *in vivo* tumor regression by ~ 2-fold compared with X-ray treatment alone (Fig. 4b).

AGuIX, small Gd-based nanoparticles designed for X-ray activation, demonstrated impressive antitumor effects in both cellular and preclinical models [74]. Compared to radiotherapy alone, AGuIX showed a 52 % increase in double-strand DNA breaks. In mice bearing multiple brain melanoma metastases, AGuIX notably extended their survival. These encouraging preclinical findings paved the way for AGuIX nanoparticles to progress into clinical trials [75,76]. Phase I trials revealed AGuIX's exemplary safety and feasibility in patients with primary melanoma, lung, breast, and colon cancers. Phase II trials showed that intravenous administration of AGuIX nanoparticles might enhance the six-month progression-free survival rate by 20 % in patients facing the most challenging prognoses [77].

4.2. X-ray-induced photodynamic therapy (X-PDT)

In X-PDT, LNPs can serve as energy transfer mediators to activate photosensitizers and produce ROS. [78]. Zhao *et al.* demonstrated that integrating porphyrin-zirconium metal–organic framework (Zr-MOF) with $NaYF_4$:Gd/Tb@$NaYF_4$ nanoparticles and rose bengal resulted in a potent 4 T1 tumor inhibition through ROS generation under X-ray irradiation [79]. Zhou *et al.* showed that the integration of Gd-doped upconversion nanoparticles with chlorin e6-embedded membrane vesicles achieved significant antitumor effects in low-dose X-ray-induced PDT [80].

Matching the emitted spectrum of LNPs upon X-ray radiation with the absorption spectrum of photosensitizers is crucial for enhancing X-PDT efficacy. Zhang *et al.* designed a nanocomposite platform using $NaGdF_4$:Tb nanoparticles and rose bengal for X-PDT [81]. The nanocomposite showcased exceptional efficiency by aligning the emission spectrum of $NaGdF_4$:Tb nanoparticles upon X-ray excitation with the absorption spectrum of rose bengal. This alignment resulted in an incredibly high Förster resonance energy transfer (FRET) efficacy of up to 99.7 %, maximizing the production of singlet oxygen crucial for PDT. When exposed to an X-ray dose of 0.6 Gy, the nanocomposite exhibited a tumor inhibition rate exceeding 90 %.

Developing new photosensitizers that directly respond to X-rays without energy transfer is an emerging strategy in X-PDT. These photosensitizers can generate electron-hole pairs that interact with the surrounding water and oxygen and produce ROS, which are responsible for the elimination of tumor cells [82]. Titanium dioxide (TiO_2) nanoparticles are widely used in LNP-mediated X-PDT for cancer therapy due to their high photocatalytic activity, excellent biocompatibility, and stability. In 2017, Yang *et al.* developed cerium (Ce)-doped TiO_2 nanoparticles for low-dose X-PDT [83]. These TiO_2:Ce nanoparticles proved more effective in generating intracellular ROS compared to TiO_2 nanoparticles alone, even at a dose of 0.12 Gy. Similarly, researchers doped europium (Eu) or gadolinium (Gd) into zinc oxide (ZnO) nanoparticles to enhance X-ray absorption [84]. The resulting Eu or Gd-doped ZnO nanoparticles exhibited a twofold increase in their ability to eliminate tumors when subjected to X-ray irradiation (2 Gy) compared to ZnO nanoparticles. This improvement is attributed to the properties of the "ejected K-shell electrons" and "photoelectron wave packets" associated with the doped nanoparticles (Fig. 4c).

Hypoxic tumors are resistant to X-rays, which may affect the clinical outcome of radiotherapy [85]. Recently, LNP-based nanoplatforms have been employed to improve the therapeutic efficacy of radiotherapy by overcoming tumor hypoxia. One effective strategy involving using small interfering RNA (siRNA), which targets hypoxic tumor cells and suppresses hypoxia-associated gene expression. For example, in 2017, Yong *et al.* developed a nanosphere radiosensitizer of chitosan-encapsulated Gd-doped polyoxometalates, loaded with hypoxia-inducible factor-1a (HIF-1a) siRNA for enhanced radiotherapy [86]. This nanocomplex improved tumor apoptosis under hypoxia conditions by 2–3 folds compared to X-ray treatment alone, thanks to siRNA's role in improving radiosensitivity. Another innovative approach is the development of oxygen-supplying LNP-based nanoplatforms to mitigate hypoxia for enhanced radiotherapy or X-PDT. In 2022, Liu *et al.* developed a core–shell nano-radiosensitizer for enhanced X-PDT by coating mesoporous silica onto $LiLuF_4$:Ce nanocrystals and embedding cerium oxide (CeO_X) nanoparticles *in situ* [87]. These nano-radiosensitizers showed potent inhibition of CT26 tumor growth under X-ray irradiation, which was attributed to the presence of CeO_X nanoparticles. The CeO_X nanoparticles show catalase-like activity and catalyze the conversion of hydrogen peroxide to water and oxygen. This reaction helps alleviate tumor hypoxia and enhance the efficacy of X-PDT.

In addition to ROS, X-ray-activated LNPs can unleash peroxynitrite ($ONOO^-$) for oncotherapy by leveraging its capacity to induce mitochondrial and DNA damage. In a recent study, Liu *et al.* developed a two-dimensional platform by combining $LiYF_4$:Ce scintillators with graphitic carbon nitride nanosheets [88]. Upon X-ray irradiation (4 Gy), this nanoplatform induced apoptosis in 4 T1 tumor cells *in vitro* and inhibited tumor growth *in vivo* by harnessing peroxynitrite-mediated DNA damage (Fig. 4d). Moreover, the same group tailored silica-coated $LiLuF_4$:Ce nanoscintillators with NO donors, g-C_3N_4 quantum dots, and polyethylene glycol (PEG) for post-surgery tumor radiotherapy [89]. In a surgical resection model of subcutaneous CT26 tumors, these nanoscintillators displayed the highest tumor growth inhibition (89.8 %) among all groups when exposed to low-dose X-rays, primarily through peroxynitrite-induced apoptosis.

Despite great progress, there are still challenges with LNP-based radiotherapy or X-PDT: i) potential damage to healthy tissues; ii) limited efficacy in transferring energy from activated LNPs to photosensitizers; iii) insufficient long-term and systemic assessment of biosafety and biocompatibility; and iv) the presence of hypoxia in the tumor microenvironment. These hurdles require further exploration and innovation to enhance the efficacy and safety of these therapies.

5. Cancer immunotherapy

Cancer immunotherapy has transformed tumor treatment, offering promising prospects for halting tumor progression, completely eliminating the tumor, preventing recurrence, and improving patient survival [90,91]. Despite their success, long-term tumor control is only achieved in a subset of patients due to various challenges, such as insufficient antitumor immune cells, diminished antigenicity in the tumor environment, and potent immunosuppression [92]. Combination therapies that leverage the strengths of different treatments provide a multifaceted approach to combat primary and metastatic tumors. LNP-based phototherapy effectively reduces surface tumor growth but struggles to completely eliminate deep-seated tumors, residual lesions, and metastases. Conversely, immunotherapy excels in eliciting strong antitumor immune responses, specifically targeting deep-seated tumors, residual lesions, and metastases [93]. Moreover, phototherapy can reverse "cold" tumors into "hot" ones, paving the way for subsequent immunotherapy to be more effective [94]. Hence, combining LNP-based phototherapy with immunotherapy can compensate for their individual

deficiencies. The principle of LNP-based cancer immunotherapy is to boost the host's cellular immunity against tumors and eliminate immunesuppressive microenvironments. In this section, we focus on lanthanide-based photoimmunotherapy, exploring the synergy between light-based therapy and immunotherapy to address these challenges.

5.1. LNP-mediated delivery of immune activators

5.1.1. Controlled release of immune activators

Immune activators, such as toll-like receptors (TLR) and stimulators of interferon genes (STING) agonists, have emerged as potent enhancers

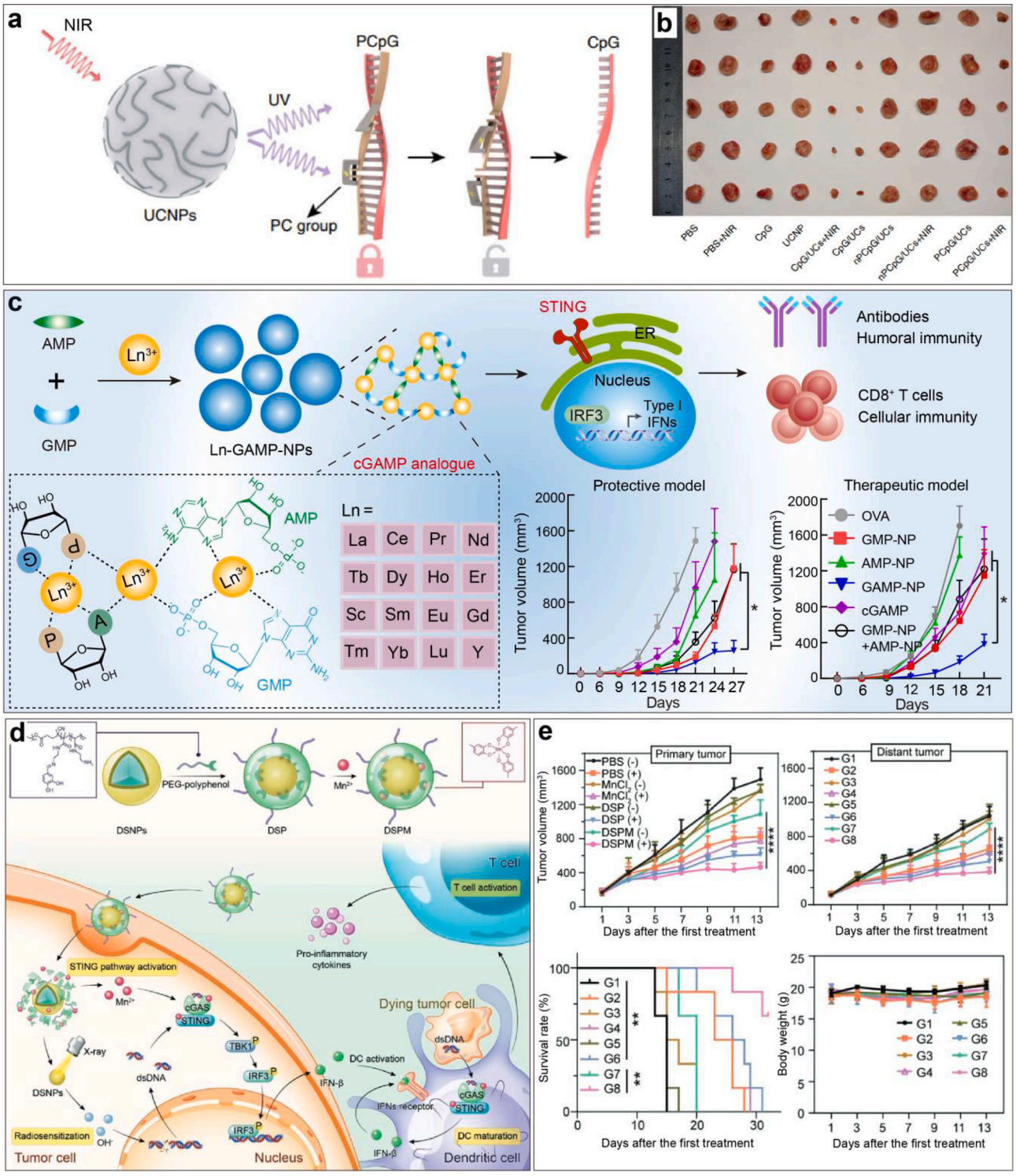

Fig. 5. LNP-based immunotherapy through the delivery of immune activators. (**a**) Mechanism of the UV light-activated immunodevice (UCNP-PCpG). (**b**) Corresponding tumor images recorded from different groups of mice on day 16 after treatment. Reproduced with permission from Ref. [97]. Copyright 2019, Springer Nature. (**c**) Lanthanide-based STING-activating coordination nanoparticles and their impact on inhibiting tumor growth in protective and therapeutic models. Reproduced with permission from Ref. [98]. Copyright 2022, American Chemical Society. (**d**) Design and working mechanism of STING-activating metal-phenolic networks. (**e**) Primary and secondary tumor growth curves, survival rates, and body weights of mice treated with different formulations. Reproduced with permission from Ref. [99]. Copyright 2022, Wiley-VCH Verlag GmbH & Co. KGaA.

of antitumor immune responses. These activators stimulate antigen-presenting cells (APCs), initiating cytotoxic T cell-mediated adaptive antitumor immunity. To protect these immune activators from degradation and ensure efficient delivery, LNPs are employed. For example, Li *et al.* prepared a novel nanoplatform using europium-doped $GdPO_4$ hollow spheres and polymer core–shell nanoparticles to co-deliver a model protein (OVA) and a TLR 9 agonist (CpG ODNs) [95]. This platform effectively shielded OVA and CpG from degradation, promoting their uptake by APCs and triggering a robust OVA-specific immune response.

5.1.2. On-demand release of immune activators

Achieving precise delivery of immune activators to tumor sites is crucial for enhancing therapeutic efficacy while minimizing systemic toxicity. LNPs offer a promising platform for optically controlled release of immune activators at specific sites and times. In 2018, Kang *et al.* encapsulated calcium regulators into mesoporous silica-coated LNPs ($NaYF_4$:Yb/Tm) to mediate NIR-controlled calcium ion modulation in macrophages, regulating phenotype polarization [96]. The NIR-driven increase or depletion in intracellular calcium ions could effectively drive macrophages into the M1 or M2 phenotype. Similarly, Chu *et al.* developed a NIR-activated immunodevice with a UV-activatable immunostimulator (PCpG) and polymer-coated $NaGdF_4$:Yb/Tm@$NaGdF_4$ nanoparticles for remote control of antitumor immunity [97]. Under 980 nm irradiation, the UV light emitted from LNPs can activate PCpG to CpG ODNs, which bind to toll-like receptor 9 (TLR9) on dendritic cells to activate the immune response (Fig. 5a). The immune system was able to stop 4 T1 tumor growth in mice without inducing a systemic cytokine storm (Fig. 5b).

5.1.3. Self-adjuvanted LNPs for immunotherapy

Nanomaterials themselves, termed as self-adjuvanted, possess the capability to enhance immune responses and create immune-active nano-formulations. LNPs, besides activating the cellular STING pathway, significantly boost antitumor immunity. In 2022, our group developed a series of 2′3′-cGAMP surrogates in nanoparticle formulations based on the reaction of adenosine monophosphate (AMP), guanosine monophosphate (GMP), and coordinating lanthanides [98]. These lanthanide-doped coordination nanoparticles (Ln-GAMP-NPs) were able to activate the STING pathway in mice and human immune cells, promoting dendritic cell maturation and augmenting MHC-I antigen presentation (Fig. 5c). Moreover, these nanovaccines significantly increased primary and secondary antigen-specific antibodies (~180 fold) in the serum of immunized mice and significantly inhibited B16-OVA tumor growth in both protective and therapeutic models. In 2022, Yan *et al.* developed a STING-activating metal-phenolic network using $NaGdF_4$:Nd@$NaLuF_4$ nanoparticles, demonstrating significant inhibition of tumor growth and prolonged survival in tumor-bearing mice [99]. Upon X-ray irradiation, LNPs acted as radiosensitizers, enhancing the sensitivity of cancer cells to X-rays and promoting cancer cell death. Meanwhile, the released Mn^{2+} within cells could facilitate STING activation and subsequently induce DC maturation. This self-adjuvanted nanoplatform significantly inhibited primary and secondary tumor growth and prolonged the survival of tumor-bearing mice (Fig. 5d and e).

5.2. Combination immunotherapy

5.2.1. Enhancing immunotherapy via LNP-mediated PDT

LNP-based PDT can induce tumor cell apoptosis and the release of tumor-associated antigens, causing antitumor immunity. Combining LNP-based PDT with immunotherapy presents an effective therapeutic strategy for tumor eradication. For instance, a multifunctional nanoplatform (UCNP-Ce6-R837) was fabricated by co-loading Ce6 and imiquimod (R837) onto polymer-coated $NaYF_4$:Yb/Er nanoparticles to induce PDT-driven antitumor immunotherapy [100]. Upon 980 nm irradiation, this platform effectively inhibited CT26 tumor growth by enhancing immunity. The combined effects of UCNP-induced PDT and R837-mediated dendritic cell maturation via the TLR-7 receptor contributed to this result. Furthermore, in combination with a cytotoxic T lymphocyte-associated antigen-4 (CTLA-4) inhibitor, this nanoplatform demonstrated the eradication of primary tumors, inhibition of metastatic tumor growth, and the induction of long-term antitumor immune memory.

In 2022, Wang *et al.* constructed nanoprobes composed of $NaYbErF_4$@$NaGdF_4$:Yb/Er@$NaGdF_4$ nanoparticles and Zr(IV)-based porphyrin MOFs for PDT [101]. Upon 980 nm irradiation, $NaLnF_4$@-MOF facilitated NIR-II imaging-guided PDT due to the generated ROS. Combined with an anti-programmed cell death-ligand 1 (αPD-L1) antibody, the probe exhibited significant antitumor immune responses (Fig. 6a and b). In another study, Yoon *et al.* fabricated multifunctional nanocomposites consisting of macrophage membrane-coated, silica-layered $NaErF_4$@$NaLuF_4$ nanoparticles, perfluorocarbon, chlorin e6, and paclitaxel for combined tumor therapy [102]. These nanocomposites enhanced PDT, releasing antigens owing to oxygen generated by the perfluorocarbon. Simultaneously, the loaded paclitaxel reprogrammed macrophages from pro-tumor (type 2, M2) to antitumor (type 1, M1), augmenting antitumor immunity. Upon 808 nm irradiation, the composite exhibited a synergistic effect in inhibiting 4 T1 tumor growth *in vivo* (Fig. 6c).

5.2.2. Enhancing immunotherapy via LNP-mediated PTT

PTT induces immunogenic cell death and releases tumor antigens within tumor sites, fostering an inflammatory tumor microenvironment. This effect can be augmented by immune activators or immune checkpoint inhibitors. Additionally, mild PTT can disrupt the extracellular matrix (ECM), decrease interstitial fluid pressure (IFP), and enhance blood perfusion within tumors, promoting immune cell infiltration, such as T cells [103]. LNP-based PTT could effectively release tumor antigens and remodel the tumor immune microenvironment, triggering robust antitumor immunity. For instance, Song *et al.* recently developed biomimetic nanoprobes encapsulating gadolinium-doped mesoporous carbon nanoparticles (Gd-MCNs) and R837 with 4 T1 tumor extracellular vesicles [104]. Under 808 nm irradiation, these nanoprobes exhibited significant inhibition of primary tumor growth and metastasis, resulting in long-term immune memory due to superior PTT efficacy and R837-mediated immune activation (Fig. 6d). Moreover, Wang *et al.* engineered an antigen-capturing nanoplatform through the self-assembly of DSPE-PEG-maleimide, indocyanine green (ICG), and rose Bengal onto $NaYF_4$:Yb/Er@$NaYF_4$:Nd nanoparticles for combined phototherapy and immunotherapy [105]. Upon NIR laser irradiation, the nanoplatform induced immunogenic cell death, stemming from the photothermal effect generated by the loaded ICG and the ROS from the loaded rose bengal.

Tumor-derived protein antigens (TDPAs) can be effectively captured by the maleimide groups on nanoparticles, thereby forming *in situ* cancer vaccines. These vaccines efficiently suppressed both primary and distant tumor growth. When combined with an anti-CTLA-4 antibody, the nanoplatform triggered a robust long-term immune response, resulting in an 83 % survival rate upon tumor rechallenge. In 2021, Xu *et al.* developed theranostic nanoplatforms, integrating $NaLuF_4$:Yb/Er@$NaLuF_4$ nanoparticles and IR-1048 dye into a lipid-aptamer nanocomplex, enhancing lung cancer detection and treatment [106]. This nanoplatform facilitated real-time monitoring of tumor metabolic activity *via* computed tomography and upconversion luminescence imaging, enabling precise tumor ablation through temperature-feedback photothermal therapy (PTT) post-irradiation with a 1064 nm laser. When combined with chimeric antigen receptor-modified natural killer (CAR NK) cells, this PTT-mediated platform significantly suppressed lung tumor growth, preventing relapse and metastasis in other organs and achieving a 100 % survival rate within 50 days post-tumor inoculation.

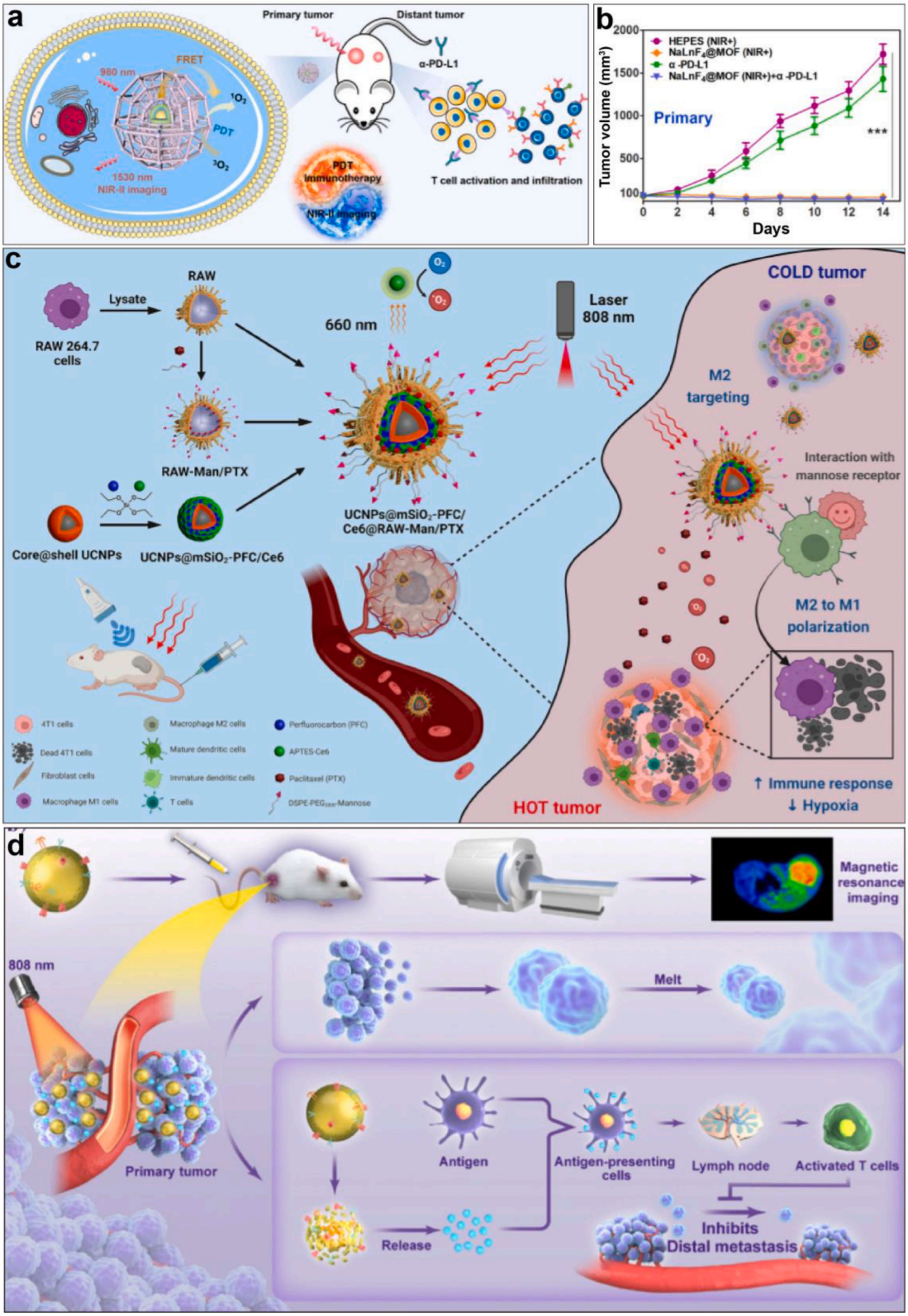

Fig. 6. Enhancing immunotherapy through LNP-mediated PDT/PTT. (**a**) $NaLnF_4$@MOF heterostructured nanoparticles designed for NIR-induced photodynamic immunotherapy. (**b**) Primary tumor growth curves of mice treated with different formulations within 14 days. Reproduced with permission from Ref. [101]. Copyright 2022, Elsevier Ltd. (**c**) Macrophage membrane-coated multifunctional nanocomposites used for NIR-driven combination therapy, which involves polarizing M2 macrophage into M1 macrophage. Reproduced with permission from Ref. [102]. Copyright 2023, Elsevier Ltd. (**d**) Biomimetic nanoprobes consisting of gadolinium-doped mesoporous carbon nanoparticles (Gd-MCNs) and R837 for photothermal-immune co-therapy. Reproduced with permission from Ref. [104]. Copyright 2023, The Royal Society of Chemistry.

5.2.2.1. Synergistic immunotherapy through LNP-based X-PDT. Compared to traditional PDT, X-PDT offers distinct advantages, such as deeper penetration and reduced tissue damage [107]. Combining X-PDT with immunotherapy enhances abscopal effects and amplifies systemic immune responses. Recent advances in LNP-based X-PDT coupled with immunotherapy have shown promise in cancer treatment. In 2021, Zhao *et al.* devised X-ray-stimulated nanoprobes comprising porphyrin Zr-based metal–organic frameworks (Zr-MOFs), $NaYF_4$:Gd/Tb@$NaYF_4$ nanoparticles, and rose bengal. These nanoprobes enabled deep-tissue PDT and synergistic immunotherapy [79]. Upon soft X-ray radiation (10–50 kV), the probe triggered ROS production at depths of about 3 cm, prompting immunogenic cell death and adaptive immune response (Fig. 7a). This combined PDT-immunotherapy significantly suppressed 4 T1 tumor growth *in vivo*. Similarly, Li *et al.* in 2021 developed $NaLuF_4$:Gd/Tb@$NaLuF_4$ nanoparticles with a photo-responsive CO-releasing moiety for synergistic CO generation and immunotherapy against 4 T1 tumors [108]. Upon X-ray exposure, the nanoplatform generated CO under blue light (475–505 nm) at deep tissues (~5 cm), enhancing ROS production, inducing immunogenic cell death, and alleviating immunosuppression (Fig. 7b). This nanovaccine effectively inhibited both primary and secondary 4 T1 tumor growth by harnessing the systemic immune response triggered by soft X-ray irradiation.

5.3. LNP-enabled light-controlled CAR T therapy

Chimeric antigen receptor (CAR) T cells, approved by the FDA since 2017 to treat leukemia and lymphoma, displayed potent treatment efficacy [109]. However, their application across other cancers is hindered by several limitations, including severe toxicities, restricted trafficking, antigen escape, and manufacturing complexities [110,111]. The utilization of LNP-enable, light-controlled CAR T therapy holds promise in mitigating some of these challenges by offering precise tumor antigen recognition [112]. For example, Nguyen *et al.* developed a tunable optogenetic nanoplatform using silica-coated $NaYbF_4$:Tm@$NaYF_4$ nanoparticles in conjunction with light-switchable CAR (LiCAR) T cells targeting CD19 protein for wireless optogenetic immunotherapy of tumors [113]. Upon 980 nm laser activation, LiCAR T cells enabled spatial and temporal control over tumor regression in B16-OVA-hCD19 tumor-bearing mice, reducing "on-target, off-tumor" effects and cytokine storm (Fig. 7c-e). This approach provided a non-invasive means to regulate CAR T cell-mediated antitumor immunity, enhancing safety and minimizing side effects. Despite notable advancements, LNP-based immunotherapy encounters challenges, including relatively low immunity induction from tumor-associated antigens, complex production procedures, limited scale of production, and insufficient systemic evaluation of long-term immune response and chronic toxicities.

6. Photo-controlled chemo/gene therapy

6.1. Photo-controlled chemotherapy

Chemotherapy, while potent against cancer, often inflicts severe adverse effects on normal tissues due to the lack of selectivity of current drugs, intrinsic drug resistance, and severe side effects [114,115]. To address these issues, various types of nanomaterial-based drug delivery systems, such as liposomes, micelles, hydrogels, or polymers, have been developed to mitigate these problems by enhancing drug pharmacokinetics [116]. However, the effect of so-called "drug burst release", in

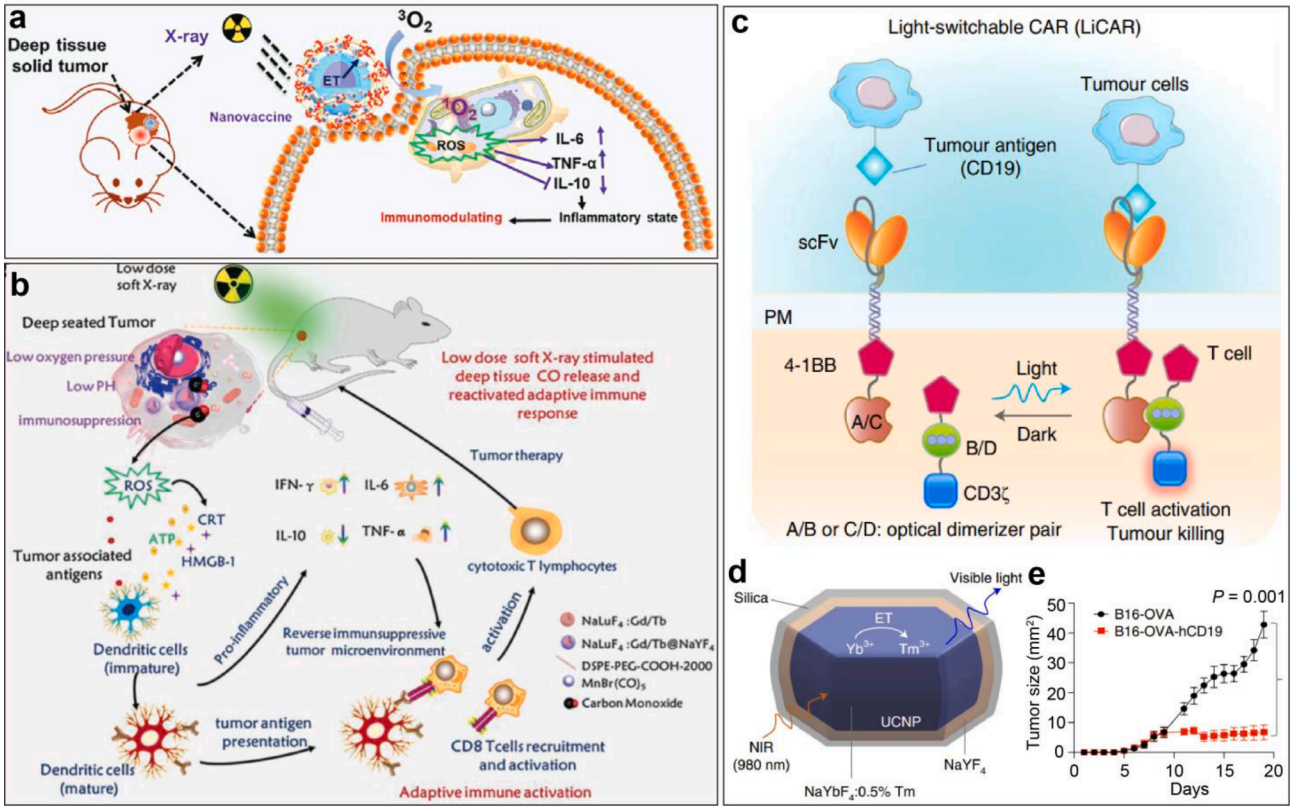

Fig. 7. Enhancing immunotherapy through LNP-based CAR T/X-PDT. (**a**) X-ray responsive nanoprobes designed for deep-tissue synergistic X-PDT and immunotherapy. Reproduced with permission from Ref. [79]. Copyright 2021, Wiley-VCH Verlag GmbH & Co. KGaA. (**b**) Photoresponsive CO-releasing nanovaccines intended for gas-sensitized and activated immunotherapy, contributing to reshaping the immunosuppressive microenvironment. Reproduced with permission from Ref. [108]. Copyright 2021, Wiley-VCH Verlag GmbH & Co. KGaA. (**c**) Photoactivatable CAR T cells, designed to activate upon exposure to light. (**d**) Design of the core–shell structure of silica-coated lanthanide nanoparticles (β-$NaYbF_4$:Tm@NaYF4). (**e**) Tumor growth curves of mice bearing B16-OVA or B16-OVA-hCD19 tumor treated with photoactivatable CAR T cells upon NIR illumination. Reproduced with permission from Ref. [113]. Copyright 2021, Springer Nature.

which some of the loaded drugs enter the bloodstream after intravenous injection, still restricts the clinical applications of these nanomedicines. Recently, *in vivo* endogenous stimuli-responsive nanomedicines have enabled highly specific cancer treatments that are less toxic than non-responsive nanomedicines. These reactions can occur in ROS-responsive moieties through oxidative stress, charge reversal of polyelectrolytes under acidic conditions, proteolysis of peptides by enzymes, or cleavage of disulfide bonds under reductive conditions. However, these stimuli-responsive delivery systems still exhibit off-target release, as these endogenous reaction processes also occur in healthy tissues [117]. Therefore, external stimuli, such as light-sensitive moieties, have received great attention in the field of chemotherapeutic delivery systems, since they can provide improved spatiotemporal control of drug release [118]. Integrating light-driven processes into chemotherapeutic systems has shown promise, primarily because light offers several advantages: it is non-invasive, its intensity and wavelength can be easily controlled, and it is straightforward to use. This innovative approach has the potential to specifically and controllably activate or release pro-drugs within tumor tissues, thereby enhancing the effectiveness of antitumor chemotherapy.

6.1.1. NIR-mediated drug delivery

One promising approach involves modifying chemotherapeutic drugs with light-responsive elements, facilitating the disintegration of nanoprobe carriers and subsequent release of chemical drugs within tumor tissues. Most recently developed light-responsive groups are sensitive to short-wavelength light, limiting their application due to shallow tissue penetration and potential phototoxicity. To address this challenge, LNPs have emerged as an exceptional option capable of harnessing NIR light and converting it into visible/UV light. This unique capability allows for the activation of photosensitive groups and controlled drug release within deeper tissue regions, presenting a potential solution for photo-responsive chemotherapy in deeply situated tumors.

For instance, Zhou *et al.* developed a NIR-responsive chemical drug delivery platform by loading Dox onto amphiphilic polymer-coated $NaYF_4$:Yb/Tm@$NaYF_4$ nanoparticles for light-triggered chemotherapy [119]. The amphiphilic polymer includes segments of poly(ethylene glycol) (PEG), pH-sensitive poly(β-aminoester), and a covalent linker of *o*-nitrobenzyl (Nbz). Upon NIR irradiation, the emission spectra of LNPs matched well with the absorption spectra of *o*-nitrobenzyl, cleaving Nbz linkers to remove PEG. This process significantly enhanced Dox's vascular extravasation and deep penetration, resulting in notable antitumor effects (Fig. 8a-c). In 2018, Hao *et al.* developed a dual-sensitive nanoplatform by co-encapsulating $NaYF_4$:Yb/Tm upconversion nanoparticles and Dox using a pH/photosensitive copolymer containing a UV–visible light-responsive cis–trans isomerism of azobenzene [120]. This nanoplatform enabled controlled Dox release, responding to both low pH conditions and NIR irradiation (980 nm), significantly enhancing cytotoxicity against HeLa tumor cells compared to Dox alone.

6.1.2. NIR-mediated pro-drug activation

LNPs are leveraged in light-triggered pro-drug activation, improving the therapeutic efficacy and reducing the toxicity of traditional chemotherapy. For instance, Li *et al.* developed magnesium silica-coated $NaYF_4$:Yb/Tm@$NaYF_4$ nanoparticles with nitric oxide (NO) precursor and Dox, countering multidrug resistance in tumors [121] (Fig. 8d). Upon 980 nm irradiation, liberated NO down-regulated resistance-related proteins, significantly enhancing Dox uptake and inhibiting multidrug-resistant tumor growth (Fig. 8e, f).

Photoreduction is another light-triggered method for converting safe pro-drugs into toxic substances. Platinum-based compounds, while effective, often exhibit strong side effects. Platinum (IV) prodrugs remain non-cytotoxic until exposed to light, activating into cytotoxic platinum (II). For instance, Dai *et al.* developed core–shell nanoparticles to activate the platinum (IV) pro-drug into toxic platinum (II) complexes through NIR irradiation [122]. This strategy, due to its deep tissue penetration, showed superior tumor inhibition compared to visible light activation. It also offered imaging-guided cancer chemotherapy. In another study, Kuang *et al.* reported multifunctional upconversion nanoprobes for multi-modal imaging and NIR-activated chemotherapy/gene therapy [123]. These nanoprobes released platinum (II) and siRNA upon 980 nm irradiation, synergistically inhibiting solid tumor growth through light-controlled drug release and gene knockdown (Fig. 8 g, h).

6.2. Light-controllable gene therapy

LNPs show promise in boosting chemotherapy and gene therapy by acting as photo-controllable nanocarriers [124]. These nanocarriers are capable of delivering various genetic cargo, such as small interfering RNA (siRNA) and clustered regularly interspaced short palindromic repeats (CRISPR)/Cas9 systems. By incorporating light-responsive elements, LNPs can precisely release loaded genes at specific target sites by harnessing external NIR light sources.

6.2.1. LNP-mediated siRNA delivery

In the realm of siRNA-based cancer therapies, effectively delivering siRNA into the cellular cytoplasm poses a challenge. LNPs offer a distinct advantage over conventional methods, enabling remote and precise gene silencing control. For instance, Zhang *et al.* developed a nanocapsule comprising mesoporous-coated $NaYF_4$:Yb/Tm@$NaYF_4$ nanoparticles, hypocrellin A (HA), PLK1 siRNA, and polyethylene glycol with photocleavable linkers for NIR-driven tumor gene therapy [125]. Upon irradiation at 980 nm, this nanocapsule notably suppressed HeLa tumor growth *in vivo* by significantly enhancing PLK1 silencing in tumor cells. Another innovation involved a photo-responsive nanocomplex encapsulating $NaYF_4$:Yb/Tm nanoparticles and PLK1 siRNA within photo-induced charge-variable cationic conjugated polyelectrolyte brushes [126]. Exposure to 980 nm irradiation triggered transformation of polymer chains, facilitating siRNA release (Fig. 9a). This nanocomplex-driven PDT and siRNA therapy efficiently inhibited HeLa tumor growth *in vivo* compared to PDT or siRNA treatment alone.

In addition, LNPs with ROS-responsive features offer an alternative for controlled siRNA release. For instance, a NIR-enhanced ROS-responsive siRNA delivery system relied on $NaYF_4$:Yb/Er@$NaYF_4$:Yb/Nd nanoparticles modified with rose bengal, PLK1 siRNA, and ROS-responsive poly(ethylenimine) containing diselenide bonds [127]. Upon 980 nm laser exposure, activated LNPs generated ROS, swiftly releasing PLK1 siRNA into cellular cytosol. This triggered effect substantially decreased PLK1 gene expression in tumor cells, significantly hindering HepG2 tumor growth (Fig. 9b).

6.2.2. LNP-mediated CRISPR/Cas9 delivery

CRISPR/Cas9 is a powerful gene-editing tool for antitumor therapy. However, conventional CRISPR/Cas9 approaches encounter hurdles in cellular uptake efficacy and off-target effects. LNPs in gene delivery offer a solution, leveraging their unique attributes to enhance the precision and efficacy of CRISPR/Cas9-mediated gene editing. In a groundbreaking study, a photo-cleavable compound (4-(hydroxymethyl)-3-nitrobenzoic acid (ONA) group) tethered the Cas9 protein to silica-coated $NaYF_4$:Yb/Tm nanoparticles [128]. This complex, armed with PLK1-targeting single-guide RNA (sgRNA) and poly(ethylenimine), responded to NIR laser irradiation by cleaving the ONA moiety. Consequently, Cas9/PLK1-sgRNA was liberated into the cytosol of A549 tumor cells, effectively impeding A549 tumor growth *in vivo* by precisely and efficiently disrupting PLK1 gene expression. This method achieved NIR-mediated remote-controlled Cas9 delivery and gene editing.

In a 2020 study, Wu *et al.* introduced a NIR-responsive CRISPR nanovector (UCNP-UVP-P). This nanovector, formed by coating UV-responsive charge-reversal conjugated polyelectrolyte polymer onto $NaYF_4$:Yb/Tm nanoparticles and loading them with PLK1-sgRNA/Cas9 plasmid through electrostatic interaction, showcased an innovative

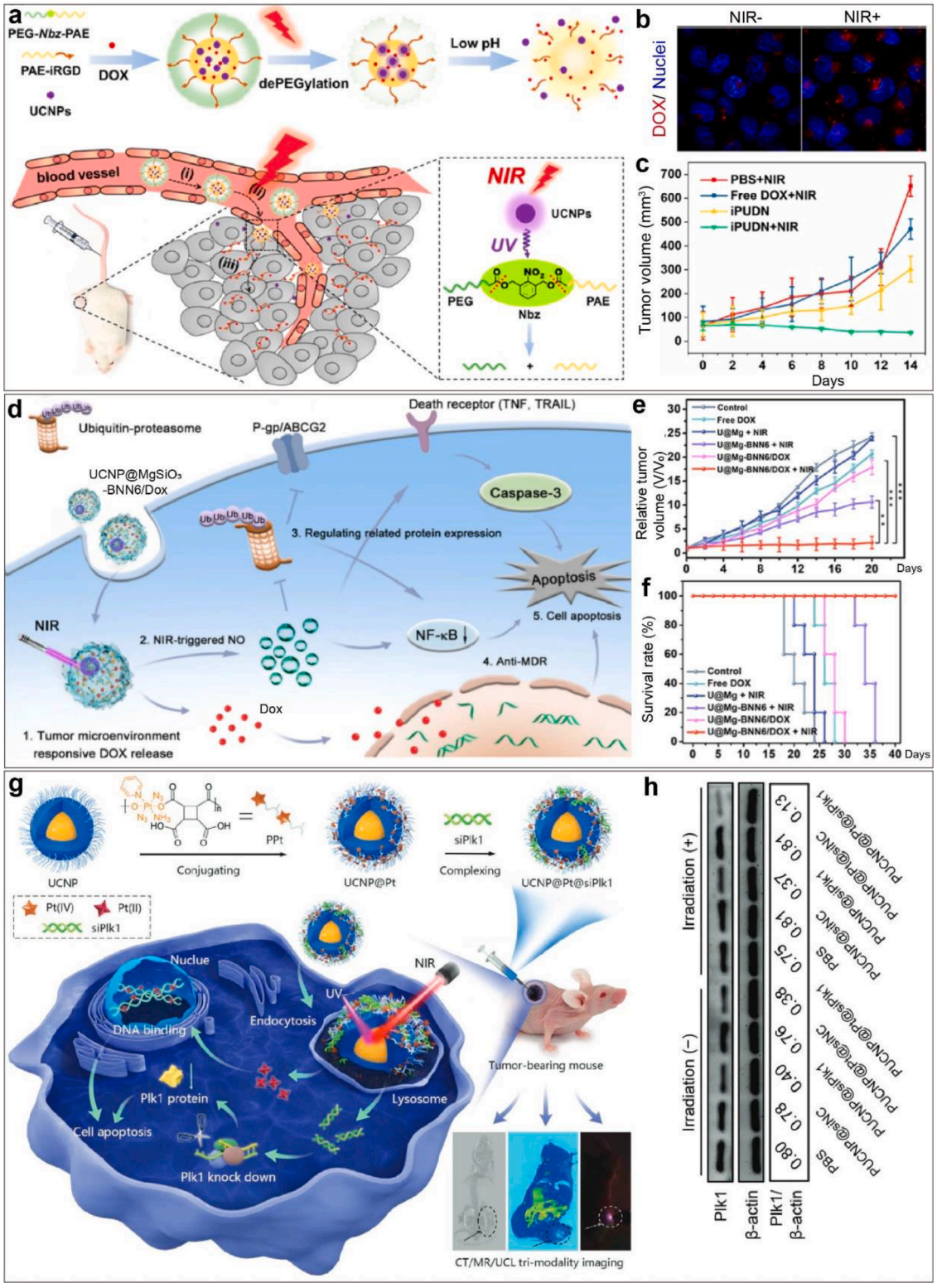

Fig. 8. LNP-enable light-controllable chemotherapy. (**a**) NIR/pH-responsive nanodrugs and their accumulation in tumor tissues. (**b**) Confocal images of MCF-7 cells incubated with nanodrugs, both under NIR irradiation and without. (**c**) Tumor growth curves of mice treated with different formulations. Reproduced with permission from Ref. [119]. Copyright 2019 American Chemical Society. (**d**) NIR-induced NO generation and NO-boosted chemotherapeutic effects of Dox on multidrug resistance tumors. **(e, f)** Tumor growth curves and survival rate of mice after different treatments. Reproduced with permission from Ref. [121]. Copyright 2020 American Chemical Society. (**g**) NIR-responsive lanthanide nanoplatform loaded with polydrug/siRNA for light-controlled delivery of chemical drugs and siRNA, along with tri-modality imaging in tumor therapy. (**h**) Western blotting analysis of PLK1 protein levels in A2780 cells after different treatments. Reproduced with permission from Ref. [123]. Copyright 2021 Wily-VCH Verlag GmbH & Co. KGaA.

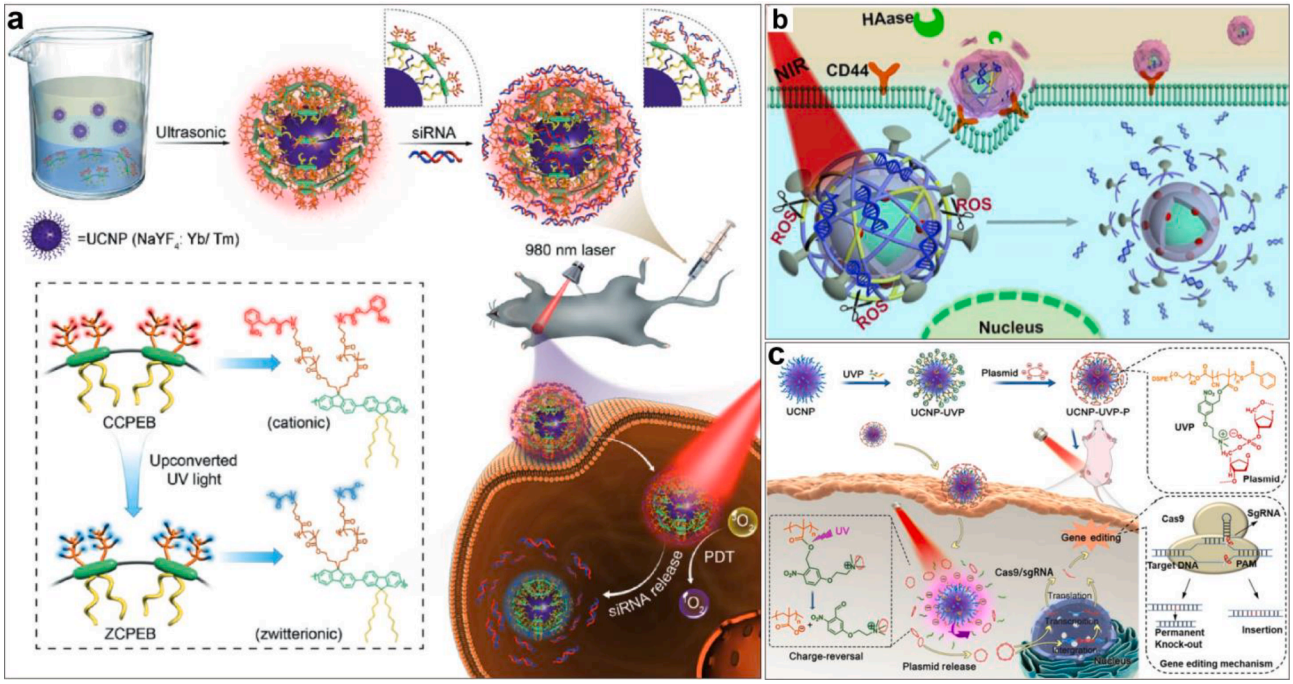

Fig. 9. LNP-enabled light-controllable gene therapy. (**a**) Photo-driven charge-variable nanoplatform designed for combined tumor PDT and siRNA therapy. Reproduced with permission from Ref. [126]. Copyright 2017 Wily-VCH Verlag GmbH & Co. KGaA. (**b**) ROS-induced sequential decomposition of the nano complex and NIR-triggered intracellular siRNA release for treatment. Reproduced with permission from Ref. [127]. Copyright 2019 Elsevier. (**c**) Schematic illustrating the preparation of a light-responsive nanovector and the NIR-triggered spatiotemporal release of CRISPR/Cas9 plasmid. Reproduced with permission from Ref. [129]. Copyright 2020 Springer Nature.

approach [129]. Under 980 nm irradiation, the nanovector transformed, transitioning to negative charges, releasing the loaded plasmids efficiently into tumor cells. Consequently, this nanovector significantly curbed HepG2 tumor growth *in vivo* by precisely and efficiently editing the PLK1 gene using the CRISPR/Cas9 system (Fig. 9c). Despite significant progress, LNP-enabled light-controlled tumor chemical/gene therapy still faces limitations in complex procedures and small-scale production.

7. Other LNP-based light-controllable treatments

7.1. Photo-controlled gas therapy

Gas-based therapy, including nitric oxide (NO), hydrogen sulfide (H_2S), sulfur dioxide (SO_2), and carbon monoxide (CO), holds promise in cancer therapy, as these gases play a key role in physiological and pathological processes [130]. Recently, LNP-based gas-generating nanoplatforms have gained attention as innovative theranostic tools for cancer therapy, offering benefits such as non-invasiveness and precise controllability. In 2015, Zhang *et al.* reported that controllable generation of NO for cancer therapy was achieved by silica-coated upconversion nanoparticles loaded with photosensitive NO donors (Roussin's black salt) upon 980 nm irradiation [131]. They also found that a high concentration of NO generated by the nanoplatform can directly kill tumor cells but the low concentration of NO can reduce the expression of P-glycoprotein by tumor cells, thereby overcoming multidrug resistance. In 2020, Li *et al.* developed a NIR-controllable NO-releasing nanoplatform consisting of magnesium silica-coated upconversion nanoparticles, an NO precursor (bis-*N*-nitroso compound-6, BNN6), and doxorubicin (DOX), for chemo/gas cancer therapy [121]. Upon 980 nm irradiation, this platform could induce apoptosis of multidrug resistant cancer cells and completely inhibit tumor growth *in vivo,* resulting from the combined effect of NO-mediated reversal of drug resistance and DOX-induced cell apoptosis.

Carbon monoxide (CO) at high cellular concentration can increase ROS content in mitochondria and suppress mitochondrial respiration, inducing tumor cell apoptosis. Therefore, LNP-activated CO release with controllability and specificity is an effective strategy for cancer therapy. A NIR-activated nanoplatform for CO generation was constructed from lipid-coated upconversion nanoparticles ($NaYF_4$:Yb/Tm@$NaYF_4$:Nd) and amphiphilic manganese carbonyl complex CO prodrug for cancer gas therapy [132]. Upon 808 nm or 980 nm laser irradiation, this nanoplatform could emit UV light to trigger CO release from the loaded prodrug and subsequently boost the generation of intracellular ROS, thereby inducing apoptosis of HCT166 tumor cells (Fig. 10a).

Similar to CO, H_2S and SO_2 gases also induce mitochondrial inhibition and cell apoptosis at high cellular concentrations. Therefore, LNP-based platforms for the generation of H_2S and SO_2 are also employed for cancer therapy. In 2019, Li *et al.* developed a NIR-triggered SO_2 generating nanoplatform for cancer therapy [133]. This platform was formed by loading SO_2 prodrug (1-(2, 5-dimethylthien-1,1-dioxide-3-yl)-2-(2,5-dimethylthien-3-yl)-hexafluorocyclopente) onto silica-coated $NaYF_4$:Yb/Tm@$NaYF_4$ nanoparticles (Fig. 10b). Under 980 nm irradiation, the UV light emitted from the nanoplatform triggers the release of SO_2, which increases intracellular ROS, thereby leading to DNA damage and cell apoptosis. This nanoplatform-based SO_2 therapy significantly inhibited the growth of S180 tumor *in vivo* and prolonged the survival rate of tumor-bearing mice. In another study, a simple NIR-triggered H_2S-generating nanocarrier was developed by loading H_2S donors, propane-2, 2-diylbis((1-(4,5-dimethoxy-2-nitrophenyl)ethyl)sulfane, SP), onto PEG-coated upconversion nanoparticles [134]. Upon 980 nm irradiation, the UV light emitted from the nanocarrier could cleave the SP molecule into *gem*-dithiols. These unstable *gem*-dithiols readily undergo hydrolysis to release H_2S, which can directly kill tumor cells. Although LNP-based gas treatments exhibit promising therapeutic efficacy in cancer therapy, these strategies are still in their infancy. More efforts should be devoted to the long-term toxicity of gas therapy *in vivo*, the release kinetics of the gas *in vivo*, and the exact therapeutic mechanism of gas therapy.

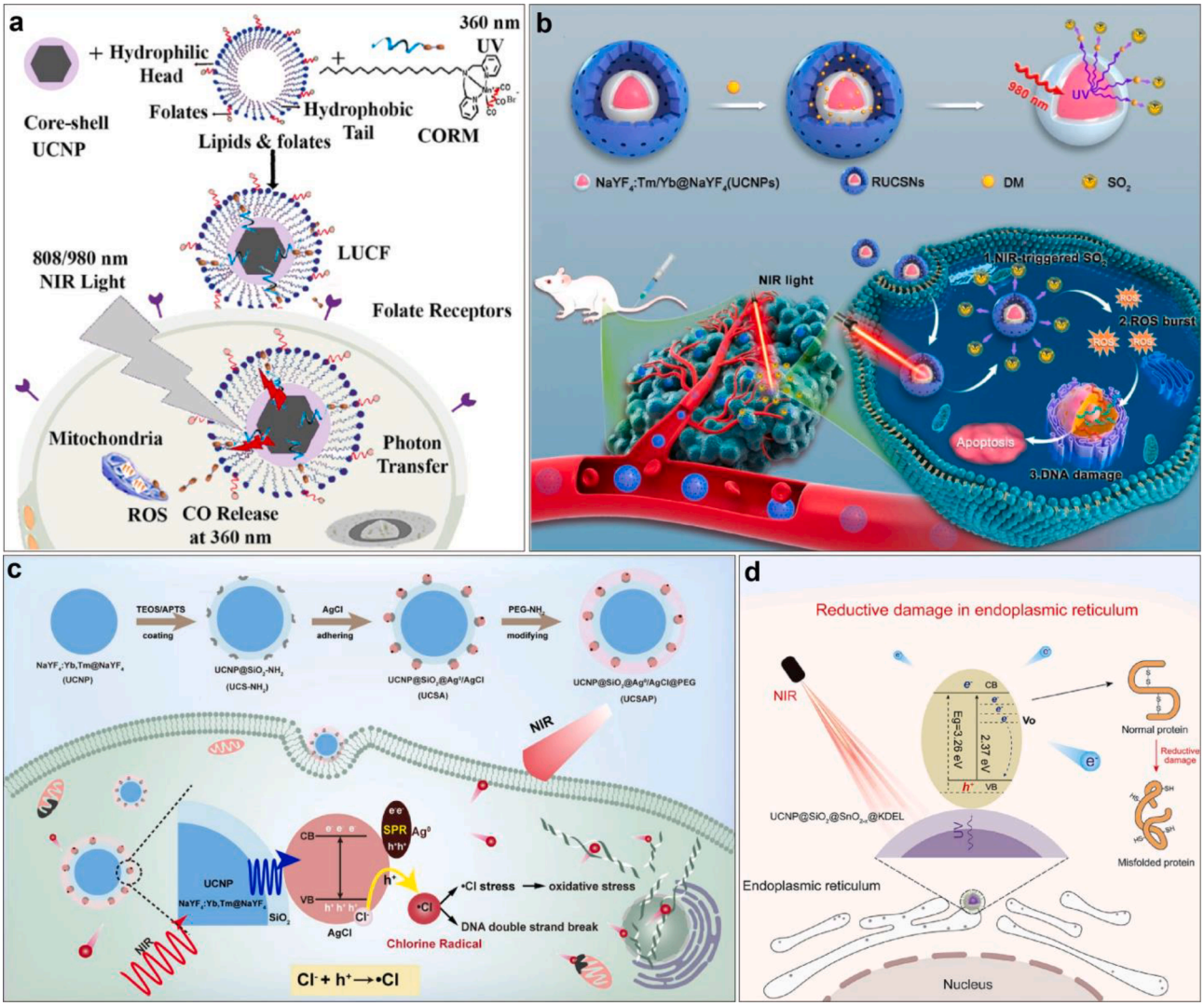

Fig. 10. LNP-based therapies utilizing light-controllable gas and non-oxygen free radical approaches. **(a)** A nanoplatform for cancer therapy through NIR-triggered intracellular CO generation. Reproduced with permission from Ref. [132]. Copyright 2020 Elsevier Ltd. (**b**) Schematic of an UNCP-based nanoplatform that releases SO_2 under NIR induction for cancer treatment. Reproduced with permission from Ref. [133]. Copyright 2019 American Chemical Society. (**c**) NIR-triggered chlorine radical stress by UCNP@Ag^0/AgCl-based nanocomplex for cancer therapy. Reproduced with permission from Ref. [135]. Copyright 2020 Wily-VCH Verlag GmbH & Co. KGaA. (**d**) Schematic of NIR-triggered cellular disruption for electronic interference in cancer therapy. Reproduced with permission from Ref. [136]. Copyright 2022, Elsevier Ltd.

7.2. Light-triggered non-oxygen free radicals for cancer therapy

In addition to ROS, light-triggered non-oxygen free radicals also can be applied to cancer therapy, since they are chemically oxidative due to unpair electrons. These free radicals can directly interact with surrounding substances such as lipids, proteins, and DNA, thereby inducing tumor cell apoptosis without causing drug-resistance. Thus, this approach addresses the common issue of oxygen deficiency in tumor sites during LNP-based tumor PDT. For example, in 2020, Song *et al.* first reported an innovative strategy based on UCNPs, a O_2-independent free radical-mediated approach, to generate chlorine radical (•Cl) stress for cancer therapy [135]. In this study, they developed a chlorine radical (•Cl) nanogenerator, which was fabricated by SiO_2-coated UCNPs as the core and Ag^0/AgCl hetero-dots as the shell. Upon 980 nm exposure, the UV light emitted from UCNPs can catalyze Ag^0/AgCl to produce •Cl, circumventing the requirement for O_2/H_2O_2. These electrophilic chlorine radicals with strong oxidizing ability exhibited enhanced efficacy in attacking biomolecules including the DNA skeleton and proteins compared to ROS, leading to severe oxidative damage in both normal and hypoxic tumors (Fig. 10c).

7.3. Light-triggered electron interference therapy

Upon NIR irradiation, LNP-based nanocomplexes can generate electrons that can destroy the oxidative state of endoplasmic reticulum (ER) and inducing apoptosis of tumor cells. Therefore, photogenerated electrons by LNP are considered a promising strategy for anticancer treatments. For instance, in 2022, Chen *et al.* designed an upconversion nanoprobe consisting of self-doped SnO_{2-X} semiconductor nanocrystals, Yb/Tm-doped upconversion nanoparticles, and the ER-targeting peptide Lys-Asp-Glu-Leu motif for electronic interference in cancer therapy [136]. Upon 980 nm excitation, the ultraviolet fluorescence generated by UCNPs could excite the separation of electron-hole pairs in the SnO_{2-X} layer, resulting in the generation of electrons (Fig. 10d). These photogenerated electrons induced apoptosis of tumor cells by disrupting the oxidative protein folding process of the endoplasmic reticulum, providing a unique strategy to induce cancer cell death.

8. Outlook

LNPs have shown potential for cancer phototherapy due to their

outstanding traits such as chemical stability and photostability, NIR excitability, and facile surface engineering for greater brightness, prolonged circulation time within the body, deep-tissue penetration, and precise tumor targeting. LNP-coupled phototherapy has proven to be a promising and minimally invasive cancer treatment due to its high therapeutic efficiency.

In recent decades, diverse LNPs have been developed for various modalities of cancer phototherapy, spanning photodynamic therapy, photothermal therapy, light-guided chemotherapy/gene therapy, radiotherapy, X-ray-induced PDT, and photoimmunotherapy. Despite great strides, there are still challenges in the clinical application of LNP-based tumor phototherapy that require special attention in future research endeavors.

Enhancing the quantum efficiency of upconversion emission, particularly in hydrophilic environments, promises to improve therapeutic outcomes in PDT and PTT. Augmenting nanoplatform brightness could enhance energy transfer to photosensitizers or photothermal agents, intensifying ROS generation or heat for tumor cell eradication. Additionally, the development of LNPs activated by NIR-II light (1000–1700 nm) is a priority due to their ability to penetrate deeper into the tissue. They are ideal for treating deep-seated tumors while minimizing heating effects.

Addressing the challenge of adequate O_2 availability in LNP-based PDT is crucial. Strategies utilizing O_2 carriers to modulate tumor hypoxia for enhanced PDT efficacy need further investigation to understand the relationship between O_2 retention, distribution, and PDT efficacy. The pursuit of O_2-independent LNP-based PDT utilizing type I photosensitizers presents another avenue for tumor cell elimination.

Scaling up the production of homogeneous LNP-based therapeutic probes with high repeatability remains a significant hurdle due to intricate procedures. Focused research into self-assembly systems may provide insights into large-scale production of controllable therapeutic LNPs, which could revolutionize cancer treatment at a reduced cost.

Assessing the biosafety, side effects, and biodegradation pathways of LNP-based nanoprobes *in vitro* and *in vivo* is critical for their clinical translation. A thorough investigation of their stability, biocompatibility, immunogenicity, pharmacokinetics, biodistribution and excretion, especially in larger animal models, is imperative prior to clinical application.

A singular phototherapy model often falls short in eradicating tumors, especially metastatic tumors. The need is to develop smart LNP-based therapeutic systems that combine various phototherapy modalities, such as PDT, PTT, immunotherapy, and X-PDT. These efforts aim to generate synergistic effects against tumors, potentially advancing the practical use of antitumor phototherapeutics in clinical settings.

CRediT authorship contribution statement

Zichao Luo: Conceptualization (lead), Writing – original draft (lead), Writing – review & editing (lead). **Duo Mao:** Writing – original draft (supporting). **Xinchao Li:** Writing – original draft (supporting). **Jing Luo:** Writing – original draft (supporting). **Changyang Gong:** Conceptualization (supporting), Writing – review & editing (supporting), Supervision (lead). **Xiaogang Liu:** Conceptualization (supporting), Funding acquisition (lead), Project administration (lead), Writing – review & editing (supporting), Supervision (lead).

Declaration of competing interest

The authors declare that they have no known competing financial interests or personal relationships that could have appeared to influence the work reported in this paper.

Data availability

No data was used for the research described in the article.

Acknowledgements

The work was supported by a National Research Foundation Singapore-Competitive Research Programme (NRF-CRP23-2019-0002), National Research Foundation, Prime Minister's Office, Singapore, under the NRF Investigatorship Programme (Award No. NRF-NRFI05-2019-0003), and NUS NANONASH Programme (NUHSRO/2020/002/NanoNash/LOA; R143000B43114).

References

[1] D.E. Dolmans, D. Fukumura, R.K.J. Jain, Nat. Rew. Cancer 3 (2003) 380–387.
[2] J. Celli, B. Spring, I. Rizvi, C. Evans, K. Samkoe, S. Verma, B. Pogue, T. Hasan, Chem. Rew. 110 (2010) 2795–2838.
[3] A. Patrizi, B. Raone, G. MRavaioli, Clin. Cosmet. Investig. Dermatol. 8 (2015) 511–520.
[4] B. Diffey, Phys. Med. Biol. 25 (1980) 405.
[5] J. Adauwiyah, H. Suraiya, Med. J. Malaysia. 65 (2010) 297–299.
[6] M. Hession, A. Markova, E. Graber, Dermatol. Surg. 41 (2015) 307–320.
[7] D. Wang, H. Wu, S. Phua, G. Yang, W. Lim, L. Gu, C. Qian, H. Wang, Z. Guo, H. Chen, Nat. Comm. 11 (2020) 357.
[8] Á. Juarranz, P. Jaén, F. Sanz-Rodríguez, J. Cuevas, S. González, Clin. Transl. Oncol. 10 (2008) 148–154.
[9] X. Li, J. Lovell, J. Yoon, X. Chen, Nat. Rew. Clin. Oncol. 17 (2020) 657–674.
[10] Z. Luo, T. He, P. Liu, Z. Yi, S. Zhu, X. Liang, E. Kang, C. Gong, X. Liu, Adv. Healthc. Mater. 10 (2021) 2002080.
[11] Y. Wang, Y. Liu, H. Sun, D. Guo, Coord. Chem. Rev. 395 (2019) 46–62.
[12] Z. Luo, Z. Yi, X. Liu, Acc. Chem. Res. 56 (2023) 425–439.
[13] M. Mitchell, M. Billingsley, R. Haley, M. Wechsler, N. Peppas, R. Langer, Nat. Rev. Drug Disov. 20 (2021) 101–124.
[14] B. Zheng, J. Fan, B. Chen, X. Qin, J. Wang, F. Wang, R. Deng, X. Liu, Chem. Rew. 122 (2022) 5519–5603.
[15] Z. Yi, Z. Luo, X. Qin, Q. Chen, X. Liu, Acc. Chem. Res. 53 (2020) 2692–2704.
[16] A. Ansari, A. Parchur, G. Chen, Coord. Chem. Rev. 457 (2022) 214423.
[17] Y. Wang, K. Zheng, S. Song, D. Fan, H. Zhang, X. Liu, Chem. Soc. Rev. 47 (2018) 6473–6485.
[18] Y. Zhong, H. Dai, Nano Res. 13 (2020) 1281–1294.
[19] J. Yan, B. Li, P. Yang, J. Lin, Y. Dai, Adv. Funct. Mater. 31 (2021) 2104325.
[20] K. Zheng, K. Loh, Y. Wang, Q. Chen, J. Fan, T. Jung, S. Nam, Y. Suh, X. Liu, Nano Today 29 (2019) 100797.
[21] G. Chen, H. Qiu, P. Prasad, X. Chen, Chem. Rev. 114 (2014) 5161–5214.
[22] M. Jafari, A. Rezvanpour, Adv. Powder Technol. 30 (2019) 1731–1753.
[23] Y. Liu, X. Meng, W. Bu, Coord. Chem. Rev. 379 (2019) 82–98.
[24] G. Tian, X. Zhang, Z. Gu, Y. Zhao, Adv. Mater. 27 (2015) 7692–7712.
[25] G. Chen, Y. Cao, Y. Tang, X. Yang, Y. Liu, D. Huang, Y. Zhang, C. Li, Q. Wang, Adv. Sci. 7 (2020) 1903783.
[26] L. Liang, Y. Lu, R. Zhang, A. Care, T. Ortega, S. Deyev, Y. Qian, A. Zvyaginacd, Acta Biomater. 51 (2017) 461–470.
[27] C. Wang, H. Tao, L. Cheng, Z. Liu, Biomaterials 32 (2011) 6145–6154.
[28] S. Cui, D. Yin, Y. Chen, Y. Di, H. Chen, Y. Ma, S. Achilefu, Y. Gu, ACS Nano 7 (2013) 676–688.
[29] M. Feng, R. Lv, L. Xiao, B. Hu, S. Zhu, F. He, P. Yang, J. Tian, Inorg. Chem. 57 (2018) 14594–14602.
[30] H. Yuan, H. Chong, B. Wang, C. Zhu, L. Liu, Q. Yang, F. Lv, S. Wang, J. Am. Chem. Soc. 134 (2012) 13184–13187.
[31] S. Bi, Z. Deng, J. Huang, X. Wen, S. Zeng, Adv. Mater. 35 (2023) 2207038.
[32] K. Pham, L. Wang, C. Hsieh, Y. Hsu, L. Chang, W. Su, Y. Chien, C. Yeh, J. Mater. Chem. B 9 (2021) 694–709.
[33] S. He, N. Johnson, V. Nguyen Huu, Y. Huang, A. Almutairi, Chem. Mater. 30 (2018) 3991–4000.
[34] B. Güleryüz, U. Ünal, M. Gülsoy, Photodiagnosis Photodyn. Ther. 36 (2021) 102616.
[35] M. Yang, H. Wang, Z. Wang, Z. Han, Y. Gu, Biomater. Sci. 7 (2019) 1686–1695.
[36] S. Lee, R. Lee, E. Kim, S. Lee, Y. Park, Front. bioeng, Biotechnol. 8 (2020) 275.
[37] S. Ding, W. Wu, T. Peng, W. Pang, P. Jiang, Q. Zhan, S. Qi, X. Wei, B. Gu, B. Liu, Nanoscale Adv. 3 (2021) 2325–2333.
[38] Y. Li, Z. Di, J. Gao, P. Cheng, C. Di, G. Zhang, B. Liu, X. Shi, L. Sun, L. Li, J. Am. Chem. Soc. 139 (2017) 13804–13810.
[39] L. He, Q. Ni, J. Mu, W. Fan, L. Liu, Z. Wang, L. Li, W. Tang, Y. Liu, Y. Cheng, J. Am. Chem. Soc. 142 (2020) 6822–6832.
[40] L. He, M. Brasino, C. Mao, S. Cho, W. Park, A. Goodwin, J. Cha, Small 13 (2017) 1700504.
[41] D. Yang, G. Yang, S. Gai, F. He, C. Li, P. Yang, ACS Appl. Mater. Inter. 9 (2017) 6829–6838.
[42] Z. Xie, X. Cai, C. Sun, S. Liang, S. Shao, S. Huang, Z. Cheng, M. Pang, B. Xing, A. Kheraif, Chem. Mater. 31 (2018) 483–490.
[43] X. Wang, J. Xu, D. Yang, C. Sun, Q. Sun, F. He, S. Gai, C. Zhong, C. Li, P. Yang, J. Chem. Eng. 354 (2018) 1141–1152.
[44] H. Sies, D. Jones, Nat. Rev. Mol. Cell Biol. 21 (2020) 363–383.
[45] C. Liu, B. Liu, J. Zhao, Z. Di, D. Chen, Z. Gu, L. Li, Y. Zhao, Angew. Chem. Int. Ed. Engl. 59 (2020) 2634–2638.
[46] F. Yu, Y. Shao, X. Chai, Y. Zhao, L. Li, Angew. Chem. Int. Ed. Engl. 61 (2022) e202203238.

[47] B. Zheng, D. Zhong, T. Xie, J. Zhou, W. Li, A. Ilyas, Y. Lu, M. Zhou, R. Deng, Chem 7 (2021) 1615–1625.
[48] F. Wei, T. Rees, X. Liao, L. Ji, H. Chao, Coord. Chem. Rev. 432 (2021) 213714.
[49] P. Wang, X. Li, C. Yao, W. Wang, M. Zhao, A. El-Toni, F. Zhang, Biomaterials 125 (2017) 90–100.
[50] C. Yao, W. Wang, P. Wang, M. Zhao, X. Li, F. Zhang, Adv. Mater. 30 (2018) 1704833.
[51] C. Zhang, W. Chen, L. Liu, W. Qiu, W. Yu, X. Zhang, Adv. Funct. Mater. 27 (2017) 1700626.
[52] Y. Chen, Y. Yang, S. Du, J. Ren, H. Jiang, L. Zhang, J. Zhu, ACS Appl. Mater. Inter. 5 (2023) 35884–35894.
[53] Y. Liu, Y. Liu, W. Bu, C. Cheng, C. Zuo, Q. Xiao, Y. Sun, D. Ni, C. Zhang, J. Liu, Angew. Chem. Int. Ed. Engl. 127 (2015) 8223–8227.
[54] X. Xue, H. Chen, Y. Xiong, R. Chen, M. Jiang, G. Fu, Z. Xi, X. Zhang, J. Ma, W. Fang, ACS Appl. Mater. Inter. 13 (2021) 4975–4983.
[55] C. Xu, K. Pu, Chem. Soc. Rev. 50 (2021) 1111–1137.
[56] K. Zhao, J. Sun, F. Wang, A. Song, K. Liu, H. Zhang, ACS Appl. Bio Mater. 3 (2020) 3975–3986.
[57] B. Liu, C. Li, B. Xing, P. Yang, J. Lin, J. Mater. Chem. B 4 (2016) 4884–4894.
[58] X. Li, M. Jiang, S. Zeng, H. Liu, Theranostics 9 (2019) 3866.
[59] X. Wang, H. Li, F. Li, X. Han, G. Chen, Nanoscale 11 (2019) 22079–22088.
[60] S. Han, A. Samanta, X. Xie, L. Huang, J. Peng, S. Park, D. Teh, Y. Choi, Y. Chang, A. All, Adv. Mater. 29 (2017) 1700244.
[61] C. Yang, L. Ma, X. Zou, G. Xiang, W. Chen, Cancer Nanotechnol. 4 (2013) 81–89.
[62] B. Liu, C. Li, Y. Chen, Y. Zhang, Z. Hou, S. Huang, J. Lin, Nanoscale 7 (2015) 1839–1848.
[63] Q. Xiao, X. Zheng, W. Bu, W. Ge, S. Zhang, F. Chen, H. Xing, Q. Ren, W. Fan, K. Zhao, J. Am. Chem. Soc. 135 (2013) 13041–13048.
[64] R. Lv, P. Yang, B. Hu, J. Xu, W. Shang, J. Tian, ACS Nano 11 (2017) 1064–1072.
[65] X. Ge, Z. Song, L. Sun, Y. Yang, L. Shi, R. Si, W. Ren, X. Qiu, H. Wang, Biomaterials 108 (2016) 35–43.
[66] K. Du, P. Lei, L. Dong, M. Zhang, X. Gao, S. Yao, J. Feng, H. Zhang, Appl. Mater. Today 18 (2020) 100497.
[67] A. Shada, L. Dengel, G. Petroni, M. Smolkin, S. Acton, C. Slingluff Jr, J. Surg. Res. 182 (2013) e9–e14.
[68] E. Carrasco, B. Del Rosal, F. Sanz-Rodríguez, A. De La Fuente, P. Gonzalez, U. Rocha, K. Kumar, C. Jacinto, J. Solé, D. Jaque, Adv. Funct. Mater. 25 (2015) 615–626.
[69] X. Zhu, W. Feng, J. Chang, Y. Tan, J. Li, M. Chen, Y. Sun, F. Li, Nat. Commun. 7 (2016) 10437.
[70] Y. Liu, X. Zhu, Z. Wei, W. Feng, L. Li, L. Ma, F. Li, J. Zhou, Adv. Mater. 33 (2021) e2008615.
[71] X. Chen, D. Peng, Q. Ju, F. Wang, Chem. Soc. Rev. 44 (2015) 1318–1330.
[72] H. Wang, X. Mu, H. He, X. Zhang, Trends Pharmacol. 39 (2018) 24–48.
[73] P. Mowat, A. Mignot, W. Rima, F. Lux, O. Tillement, C. Roulin, M. Dutreix, D. Bechet, S. Huger, L. Humbert, J. Nanosci. Nanotechnol. 11 (2011) 7833–7839.
[74] S. Kotb, A. Detappe, F. Lux, F. Appaix, E.L. Barbier, V. Tran, M. Plissonneau, H. Gehan, F. Lefranc, C. Rodriguez-Lafrasse, Theranostics 6 (2016) 418.
[75] C. Verry, S. Dufort, B. Lemasson, S. Grand, J. Pietras, I. Troprès, Y. Crémillieux, F. Lux, S. Mériaux, B. Larrat, Sci. Adv. 6 (2020) eaay5279.
[76] C. Verry, S. Dufort, J. Villa, M. Gavard, C. Iriart, S. Grand, J. Charles, B. Chovelon, J. Cracowski, J. Quesada, Radiother. Oncol. 160 (2021) 159–165.
[77] E. Thivat, M. Casile, J. Moreau, I. Molnar, S. Dufort, K. Seddik, G. Le Duc, O. De Beaumont, M. Loeffler, X. Durando, Radiother. Oncol. 23 (2023) 344.
[78] Z. Hong, Z. Chen, Q. Chen, H. Yang, Acc. Chem. Res. 56 (2022) 37–51.
[79] X. Zhao, Y. Li, L. Du, Z. Deng, M. Jiang, S. Zeng, Adv. Healthc. Mater. 10 (2021) 2101174.
[80] D. Zhou, Y. Gao, Z. Yang, N. Wang, J. Ge, X. Cao, D. Kou, Y. Gu, C. Li, M. Afshari, ACS Appl. Mater. Inter. 15 (2023) 26431–26441.
[81] W. Zhang, X. Zhang, Y. Shen, F. Shi, C. Song, T. Liu, P. Gao, B. Lan, M. Liu, S. Wang, Biomaterials 184 (2018) 31–40.
[82] H. Wang, B. Lv, Z. Tang, M. Zhang, W. Ge, Y. Liu, X. He, K. Zhao, X. Zheng, M. He, Nano Lett. 18 (2018) 5768–5774.
[83] C. Yang, Y. Sun, P. Chung, W. Chen, W. Swieszkowski, W. Tian, F. Lin, Ceram. Int. 43 (2017) 12675–12683.
[84] B. Ghaemi, O. Mashinchian, T. Mousavi, R. Karimi, S. Kharrazi, A. Amani, ACS Appl. Mater. Inter. 8 (2016) 3123–3134.
[85] M. Horsman, L. Mortensen, J. Petersen, M. Busk, J. Overgaard, Nat. Rev. Clin. Oncol. 9 (2012) 674–687.
[86] Y. Yong, C. Zhang, Z. Gu, J. Du, Z. Guo, X. Dong, J. Xie, G. Zhang, X. Liu, Y. Zhao, ACS Nano 11 (2017) 7164–7176.
[87] S. Liu, L. Fang, H. Ding, Y. Zhang, W. Li, B. Liu, S. Dong, B. Tian, L. Feng, P. Yang, ACS Nano 16 (2022) 20805–20819.
[88] S. Liu, W. Li, H. Chen, J. Zhou, S. Dong, P. Zang, B. Tian, H. Ding, S. Gai, P. Yang, ACS Nano 16 (2022) 8939–8953.
[89] S. Liu, W. Li, Y. Zhang, J. Zhou, Y. Du, S. Dong, B. Tian, L. Fang, H. Ding, S. Gai, Nano Lett. 22 (2022) 6409–6417.
[90] K. Hiam-Galvez, B. Allen, M. Spitzer, Nat. Rew. Cancer 21 (2021) 345–359.
[91] Z. Luo, X. Liu, Next Nanotechnol. 1 (2023) 100006.
[92] A. Weverwijk, K. Visser, Nat. Rew. Cancer 23 (2023) 193–215.
[93] Z. Xie, T. Fan, J. An, W. Choi, Y. Duo, Y. Ge, B. Zhang, G. Nie, N. Xie, T. Zheng, Chem. Soc. Rev. 49 (2020) 8065–8087.
[94] J. Nam, S. Son, K.S. Park, W. Zou, L.D. Shea, J. Moon, Nat. Rev. Mater. 4 (2019) 398–414.
[95] Z. Li, Z. Liu, M. Yin, X. Yang, J. Ren, X. Qu, Adv. Healthc. Mater. 2 (2013) 1309–1313.
[96] H. Kang, K. Zhang, D.S.H. Wong, F. Han, B. Li, L. Bian, Biomaterials 178 (2018) 681–696.
[97] H. Chu, J. Zhao, Y. Mi, Z. Di, L. Li, Nat. Commun. 10 (2019) 2839.
[98] Z. Luo, X. Liang, T. He, X. Qin, X. Li, Y. Li, L. Li, X. Loh, C. Gong, X. Liu, J. Am. Chem. Soc. 144 (2022) 16366–16377.
[99] J. Yan, G. Wang, L. Xie, H. Tian, J. Li, B. Li, W. Sang, W. Li, Z. Zhang, Y. Dai, Adv. Mater. 34 (2022) 2105783.
[100] J. Xu, L. Xu, C. Wang, R. Yang, Q. Zhuang, X. Han, Z. Dong, W. Zhu, R. Peng, Z. Liu, ACS Nano 11 (2017) 4463–4474.
[101] Q. Wang, Y. Yang, X. Yang, Y. Pan, L. Sun, W. Zhang, Y. Shao, J. Shen, J. Lin, L. Li, Nano Today 43 (2022) 101439.
[102] J. Yoon, X. Le, J. Kim, H. Lee, N. Nguyen, W. Lee, E. Lee, K. Oh, H. Choi, Y. Youn, J. Control. Release 360 (2023) 482–495.
[103] X. Wang, H. Zhang, X. Chen, C. Wu, K. Ding, G. Sun, Y. Luo, D. Xiang, Acta Biomater. 166 (2023) 42–68.
[104] X. Song, C. Zhang, M. Xing, C. He, D. Wang, L. Chong, X. Zhang, M. Chen, J. Li, J. Mater. Chem. B 11 (2023) 6147–6158.
[105] M. Wang, J. Song, F. Zhou, A. Hoover, C. Murray, B. Zhou, L. Wang, J. Qu, W. Chen, Adv. Sci. 6 (2019) 1802157.
[106] M. Xu, B. Xue, Y. Wang, D. Wang, D. Gao, S. Yang, Q. Zhao, C. Zhou, S. Ruan, Z. Yuan, Small 17 (2021) 2101397.
[107] W. Sun, Z. Zhou, G. Pratx, X. Chen, H. Chen, Theranostics 10 (2020) 1296.
[108] Y. Li, M. Jiang, Z. Deng, S. Zeng, J. Hao, Adv. Sci. 8 (2021) 2004391.
[109] R.C. Larson, M. Maus, Nat. Rev. Cancer 21 (2021) 145–161.
[110] S. Rafiq, C. Hackett, R. Brentjens, Nat. Rev. Clin. Oncol. 17 (2020) 147–167.
[111] S. Neelapu, S. Tummala, P. Kebriaei, W. Wierda, C. Gutierrez, F. Locke, K. Komanduri, Y. Lin, N. Jain, N. Daver, Nat. Rev. Clin. Oncol. 15 (2018) 47–62.
[112] E. Morris, S. Neelapu, T. Giavridis, M. Sadelain, Nat. Rev. Immounol. 22 (2022) 85–96.
[113] N. Nguyen, K. Huang, H. Zeng, J. Jing, R. Wang, S. Fang, J. Chen, X. Liu, Z. Huang, M. You, Nat. Nanotechnol. 16 (2021) 1424–1434.
[114] S. Hossen, M. Hossain, M. Basher, M. Mia, M. Rahman, M. Uddin, J. Adv. Res. 15 (2019) 1–18.
[115] J. Liu, W. Bu, L. Pan, J. Shi, Angew. Chem. Int. Ed. Engl. 125 (2013) 4471–4475.
[116] Q. Yin, J. Shen, Z. Zhang, H. Yu, Y. Li, Adv. Drug. Deliv. Rev. 65 (2013) 1699–1715.
[117] X. Wang, Z. Xuan, X. Zhu, H. Sun, J. Li, Z. Xie, J. Nanobiotechnology 18 (2020) 1–19.
[118] M. Karimi, P. Sahandi Zangabad, S. Baghaee-Ravari, M. Ghazadeh, H. Mirshekari, M. Hamblin, J. Am. Chem. Soc. 139 (2017) 4584–4610.
[119] M. Zhou, H. Huang, D. Wang, H. Lu, J. Chen, Z. Chai, S. Yao, Y. Hu, Nano Lett. 19 (2019) 3671–3675.
[120] W. Hao, D. Liu, Y. Wang, X. Han, S. Xu, H. Liu, Colloids Surf. A Physicochem. Eng. Asp. 537 (2018) 446–451.
[121] S. Li, X. Song, W. Zhu, Y. Chen, R. Zhu, L. Wang, X. Chen, J. Song, H. Yang, ACS Appl. Mater. Inter. 12 (2020) 30066–30076.
[122] Y. Dai, H. Xiao, J. Liu, Q. Yuan, P. Ma, D. Yang, C. Li, Z. Cheng, Z. Hou, P. Yang, J. Lin, J. Am. Chem. Soc. 135 (2013) 18920–18929.
[123] G. Kuang, H. Lu, S. He, H. Xiong, J. Yu, Q. Zhang, Y. Huang, Adv. Healthc. Mater. 10 (2021) 2100938.
[124] M. Sohrabi, Z. Babaei, V. Haghpanah, B. Larijani, A. Abbasi, M. Mahdavi, Biomed. Pharmacother. 156 (2022) 113872.
[125] Y. Zhang, K. Ren, X. Zhang, Z. Chao, Y. Yang, D. Ye, Z. Dai, Y. Liu, H. Ju, Biomaterials 163 (2018) 55–66.
[126] H. Zhao, W. Hu, H. Ma, R. Jiang, Y. Tang, Y. Ji, X. Lu, B. Hou, W. Deng, W. Huang, Q. Fan, Adv. Funct. Mater. 27 (2017) 1702592.
[127] Y. He, S. Guo, L. Wu, P. Chen, L. Wang, Y. Liu, H. Ju, Biomaterials 225 (2019) 119501.
[128] Y. Pan, J. Yang, X. Luan, X. Liu, X. Li, J. Yang, T. Huang, L. Sun, Y. Wang, Y. Lin, Sci. Adv. 5 (2019) eaav7199.
[129] Y. Wu, J. Zheng, Q. Zeng, T. Zhang, D. Xing, Nano Res. 13 (2020) 2399–2406.
[130] N. Yang, F. Gong, L. Cheng, Chem. Sci. 13 (2022) 1883–1898.
[131] X. Zhang, G. Tian, W. Yin, L. Wang, X. Zheng, L. Yan, J. Li, H. Su, C. Chen, Z. Gu, Adv. Funct. Mater. 25 (2015) 3049–3056.
[132] Y. Opoku-Damoah, R. Zhang, H. Ta, D. Jose, R. Sakla, Z. Xu, Eur. J. Pharm. Biopharm. 158 (2021) 211–221.
[133] S. Li, R. Liu, X. Jiang, Y. Qiu, X. Song, G. Huang, N. Fu, L. Lin, J. Song, X. Chen, ACS Nano 13 (2019) 2103–2113.
[134] W. Chen, M. Chen, Q. Zang, L. Wang, F. Tang, Y. Han, C. Yang, L. Deng, Y. Liu, Chem. Commun. 51 (2015) 9193–9196.
[135] R. Song, H. Wang, M. Zhang, Y. Liu, X. Meng, S. Zhai, C. Wang, T. Gong, Y. Wu, X. Jiang, Angew. Chem. Int. Ed. Engl. 59 (2020) 21032–21040.
[136] L. Chen, X. Jiang, M. Lv, X. Wang, P. Zhao, M. Zhang, G. Lv, J. Wu, Y. Liu, Y. Yang, Chem 8 (2022) 866–879.